Geophys. J. Int. (1998) **132,** 412–434

Advection of plumes in mantle flow: implications for hotspot motion, mantle viscosity and plume distribution

Bernhard Steinberger* and Richard J. O'Connell

Department of Earth and Planetary Sciences, Harvard University, 20 *Oxford Street, Cambridge* MA 02138, *USA.*
E-mail: steinber@geophysik.uni-frankfurt.de

Accepted 1997 September 12. Received 1997 August 25; in original form 1996 August 26

SUMMARY

Because of their slow relative motion, hotspots, mainly in the Pacific, are often used as a reference frame for defining plate motions. A coherent motion of all Pacific hotspots relative to the deep mantle may, however, bias the hotspot reference frame. Numerical results on the advection of plumes, which are thought to cause the hotspots on the Earth's surface, in a large-scale mantle flow field are therefore presented. Bringing the results into agreement with observations also leads to conclusions regarding the viscosity structure of the Earth's mantle, as well as the sources and distribution of plumes.

The abrupt change in direction of the Hawaiian–Emperor chain implies an upper-mantle viscosity under the Pacific of $\sim 1.5 \times 10^{20}$ Pa s or less. Slow relative motion of hotspots requires high lower-mantle viscosity, unless hotspots are located at large-scale stationary upwellings that are currently unresolved by seismic tomography. For our preferred model, we obtain coherent motion of Pacific hotspots in a reference frame of no net rotation, as well as coherent motion relative to African hotspots, caused by return flow antiparallel to plate motion. Advection and regional differences in life expectancy can to a large part explain the distribution of plumes in relation to ridges, subduction zones (present and past) and seismic anomalies. Plume conduits are substantially tilted in the lower mantle. The surface motion of hotspots is often smaller than the advection rate of plume conduits in the lowermost mantle.

Key words: advection, hotspots, mantle convection, mantle viscosity, plume, seismic tomography.

1 INTRODUCTION

1.1 Overview

Hotspots are often used as reference points relative to which tectonic plate motions can be defined. Our main goal is to achieve a better understanding of their motion or fixity. We will therefore present numerical results regarding the motion of hotspots caused by mantle flow. Comparison with observations will also yield some new insights into the old problem of mantle viscosity. Before we start this undertaking, we will explain terms and concepts on which this work is based, in particular the following:

(1) what a hotspot is and what it is believed to be caused by;
(2) why hotspots are used as a reference frame for plate motions, and what the problems are with this reference frame;
(3) what other reference frames there are for plate motions, and how they are related.

We will do this in the context of a literature review to show the evolution of the present ideas. At appropriate points we will indicate how this work will contribute to the further development of these ideas. Our own results will then be described in detail in the following sections.

After having stated our plume model, we will present some analytical results, including a simple model which exhibits advection of plumes in a direction opposite to plate motion, and a discussion of the circumstances under which we expect that a strong tilt of the plume conduit leads to extinction of a hotspot. We will then proceed to a more realistic numerical model. Starting with time-independent kinematic flow only, we will then introduce time dependence of plate velocities, followed by models that also include density-driven flow and advection of density heterogeneities. Here we will introduce our 'preferred' model with a viscosity structure and velocity–density scaling factor such that calculated and observed

* Now at: Institut für Meteorologie und Geophysik, Universität Frankfurt, Feldbergstr. 47, 60323 Frankfurt, Germany.

GJI000 21/1/98 16:12:05 3B2 version 5.20
The Charlesworth Group, Huddersfield 01484 517077

hotspot tracks approximately agree. This model exhibits a coherent motion of hotspots opposite to plate motion and predicts a global hotspot distribution similar to what is observed. We will then present a few models that do not fit observations, and in this way constrain some of the model parameters.

1.2 Plumes and hotspots

Areas of intraplate volcanism (e.g. Hawaii), as well as especially vigorous volcanism along plate boundaries (e.g. Iceland), are referred to as *hotspots*. Active hotspot volcanism is typically constrained to a rather small area (of the order of 100 km in diameter), therefore hotspots are believed to be caused by *mantle plumes*, rather narrow upwellings in the Earth's mantle. The relative motion of hotspots appears to be much less than the relative motion of plates, therefore they are often used as a reference frame for defining plate motion.

It was Wilson (1963) who invoked a rather stationary upwelling under a moving plate in order to explain the linear age progression along volcanic island chains such as the Hawaiian islands. Dietz & Holden (1970), followed by many others, used such an upwelling or 'hotspot' as a reference point for defining plate motions, and Morgan (1971) showed that Pacific island chains can in fact be created by moving a rigid plate over stationary hotspots. Fig. 1 shows calculated hotspot tracks, assuming fixed sources, and observed island and seamount chains in the Pacific with radiometric age data. Only tracks with recently active volcanism (during the past 1 Myr) and an extended period of activity (> 10 Myr) are shown. Morgan proposed that these hotspots are caused by stationary upwellings in the lower mantle, which he termed 'plumes'.

Such plumes have also been observed in laboratory experiments, such as that of Whitehead & Luther (1975). If the viscosity inside the upwelling is smaller than that outside, they describe the shape as a 'spherical pocket of fluid fed by a pipe' (Fig. 2a), which subsequently became the standard plume model. The impinging of the roughly spherical 'plume head' on the Earth's lithosphere has been associated with flood basalts (Richards, Duncan & Courtillot 1989), whereas the remaining conduit may create a hotspot track. Richards *et al.* (1989) also attempted to match each flood basalt with a hotspot (active or extinct), and, from the extent of the flood basalts and experimental results, estimated the diameter of a plume head to be at least several hundred kilometres, whereas the diameter of the conduit is much smaller than this.

Manga, Stone & O'Connell (1993) describe the shape of plumes for a range of parameters, as obtained from both laboratory experiments and numerical calculations. Mantle plumes have also been proposed on theoretical grounds by Loper & Stacey (1983). They note that 'not only are plumes a necessary consequence of a thermal boundary layer, but their existence is impossible without that layer'. Following Morgan (1972), this boundary layer has mostly been identified as the thermal boundary layer at the core–mantle boundary (CMB).

Apart from dynamical arguments, chemical arguments have also led to this view. Chemical differences in the magmas of hotspot volcanism and ocean ridge volcanism led Anderson (1975) to conclude that hotspots originate from a chemically distinct layer D″ at the base of the mantle. Alternatively, McKenzie & O'Nions (1983) present a geochemical argument suggesting the boundary between the upper and lower mantle as a possible source region of mantle plumes.

While some regions of intraplate volcanism (such as Hawaii and Yellowstone) and of extensive volcanism along plate boundaries (e.g. Iceland and Tristan da Cunha) are generally viewed as caused by a mantle plume, the proposed total number of mantle plumes varies largely between authors. Morgan (1971) used 16 hotspots, whereas Burke & Wilson (1976) showed 122 hotspots, and Richards, Hager & Sleep (1988) compiled a list of 47 hotspots. In the following we will refer to these 47 hotspots, plus Louisville at the location given by Lonsdale (1988), as 'actual' hotspots.

A major shortcoming of the concept of plumes is that plume conduits cannot be 'seen' by seismic tomography or other means, which leaves their region of origin and their exact number uncertain.

Due to its large size, the plume head may rise rather rapidly through mantle material. The flow in a solid such as the Earth's mantle is due to dislocation creep and the relationship between stress σ and strain rate $\dot{\varepsilon}$ is thus non-linear. A relationship of the form $\dot{\varepsilon} \sim \sigma^n$ with $n > 1$ is expected. Because the rise of a plume head is associated with comparatively large stresses, the speed of rising may be further increased compared to a Newtonian fluid with $\dot{\varepsilon} \sim \sigma$ (Weinberg & Podladchikov 1994; Anderson 1981). Rising speed may also be increased due to the higher temperature and hence reduced viscosity associated with a plume head. Therefore, the plume head should move almost vertically up through the mantle and establish a rather straight conduit behind it. The low-density material in the conduit will make it buoyant in the surrounding mantle. While material may rise through the conduit much faster than the large-scale flow in the lower mantle, the buoyant rising velocity of conduit segments is likely to be rather slow, owing to their small size. Consequently, conduit segments will be advected in a large-scale mantle flow field, the conduit will be distorted, and the hotspot may move (Richards & Griffiths 1988; Griffiths & Richards 1989; see Fig. 2c) relative to other hotspots. Whitehead (1982) pointed out that a conduit will become unstable and eventually split up into separate drops if it gets distorted too strongly (Fig. 2d). He gives a critical angle of 60° with the vertical for instability to occur.

We will present results on how a plume conduit gets distorted in a mantle flow field. In many cases, the calculated shape of plume conduits will exhibit angles larger than 60° with the vertical. We will argue that this only matters for a certain viscosity range of the surrounding mantle.

1.3 Earth reference frames

Three points fixed relative to each other are sufficient to define a reference frame in 3-D space. Using these three points, a coordinate system can be defined and the location of all other points at all times can be described in the coordinate system. For a rigid body, it is possible to define a reference frame fixed to the body. Since no part of the Earth is rigid, it is more difficult to devise a suitable reference frame over geological time.

1.3.1 Hotspot reference frame

The lower mantle probably comes closest to being rigid, that is it is the region of the Earth with the slowest relative

GJI000 21/1/98 16:14:10 3B2 version 5.20
The Charlesworth Group, Huddersfield 01484 517077

Figure 1. Hotspot tracks on the Pacific Plate. Topographic relief, age data and calculated tracks (Easter: 10–68 Ma; all others: 0–68 Ma) with 10 Myr tick-mark interval using the fixed hotspot hypothesis. Numbers in brackets indicate sources of age data: (1) Duncan & Clague (1985); (2) Jarrard & Clague (1977); (3) Clague & Dalrymple (1989); (4) Desonie & Duncan (1990); (5) Johnson & Embley (1990); (6) Watts *et al.* (1988); (7) O'Connor, Stoffers & McWilliams (1995). (1)–(3) are compilations of earlier data. Assumed present locations for Caroline hotspot according to Richards *et al.* (1988), for Louisville according to Lonsdale (1988), otherwise at the presently or recently active volcanoes in italics. Plate velocities are according to Gordon & Jurdy (1986) and Lithgow-Bertelloni (1994). Shaded relief is from ETOPO5 data (National Geophysical Data Center 1988). This figure and several others were made using GMT graphics (Wessel & Smith 1991).

motion. Hotspots are believed to originate from the lower mantle and are therefore widely used as an Earth reference frame over geological time. Two hotspots fixed relative to each other at a constant angular distance would be necessary and sufficient to define a reference frame, since the centre of mass of the Earth can serve as the third point. The two most suitable hotspots are Hawaii and Louisville, since they are both associated with well-defined narrow island chains, both on the Pacific Plate, and reliable age data are available from both chains.

Even though plumes under one plate may show little relative motion, they may move relative to plumes under another plate. Olson (1987) suggested that plumes may move in a direction nearly opposite to plate motion owing to a return flow in the lower mantle. Thus there may be a coherent motion of plumes under one plate, biasing the hotspot reference frame. This effect

GJI000 21/1/98 16:14:29 3B2 version 5.20
The Charlesworth Group, Huddersfield 01484 517077

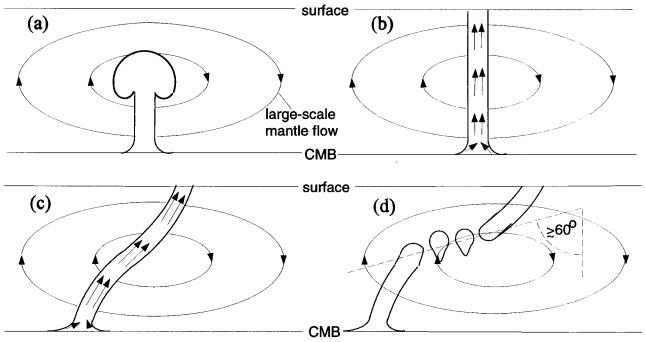

Figure 2. Four stages in the life of a mantle plume. (a) A rising plume consists of a plume head and a conduit. (b) After the plume head is erupted, the conduit is left behind. (c) A plume conduit gets distorted by mantle shear flow. (d) It splits up into several drops once the distortion gets too strong.

is illustrated in a schematic fashion in Fig. 3 and should be especially important for the Pacific Plate, since it moves very fast, and Pacific hotspots define the hotspot reference frame to a large extent.

Morgan (1981, 1983) and Duncan (1981) concluded that the relative motion of hotspots in the Atlantic and Indian Oceans is too small to be observable. Molnar & Stock (1987), however, found a motion of the Hawaiian hotspot relative to hotspots in the Atlantic and Indian Oceans of about 1 to 2 cm per year over the last 50 to 65 Myr and concluded that hotspots do not define a fixed reference frame.

It seems paradoxical that there can be fixed hotspots in a convecting mantle. Richards (1991) had concluded from numerical calculations that in the case of whole-mantle convection a substantial increase in viscosity is required in the lower mantle to ensure that relative motion between hotspots is confined to approximately an order of magnitude less than fast plate motions. Here we will present the results of a more realistic computer model to show under what circumstances the observed hotspot tracks and the apparent hotspot fixity can be reconciled with a convecting mantle. It will again turn out that this requires a rather high viscosity in the lower mantle. Also, we will show that a relative motion of hotspots on different plates can be expected.

1.3.2 Mean lithospheric reference frame

Obviously any rigid lithospheric plate can serve as a reference frame, but this is a rather arbitrary choice. A more meaningful choice is the 'mean lithosphere'. By definition, there is no net rotation of the lithosphere in the 'mean lithospheric reference frame':

$$\int \mathbf{v} \times \mathbf{r}\, dA = 0\,, \tag{1}$$

where $\mathbf{v}$ is velocity, $\mathbf{r}$ is position, the Earth's centre of mass is the origin of the coordinate system and integration extends over the whole Earth surface.

1.3.3 Tisserand's mean axes of the body

While the previous reference frame only refers to the surface of the Earth and is thus tied to observations, it is possible to define an analogous reference frame for the entire Earth or any region

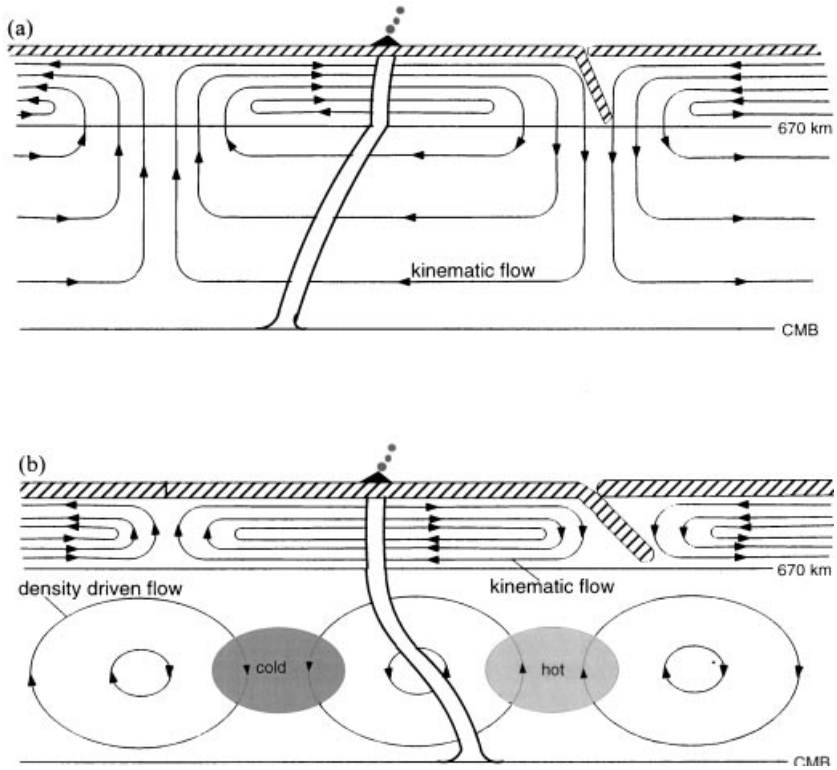

Figure 3. (a) Kinematic (plate-driven) return flow in the lower mantle may lead to a coherent motion of plumes under one plate. (b) If the viscosity in the upper mantle is very low, this effect disappears.

of it: 'Tisserand's mean axes of the body' is defined such that

$$\int \rho \mathbf{v} \times \mathbf{r} dV = 0\,, \tag{2}$$

where ρ is density. O'Connell, Gable & Hager (1991) showed that for a lateral variation in viscosity a rotation of the lithosphere relative to Tisserand's mean axes of the body is possible. The flow calculations in this work are carried out for radial variation in viscosity only and thus there can be no such rotation. We will call this reference frame in which calculations are performed the 'no-net-rotation' reference frame; hotspot motions will always be plotted in this reference frame. For the purpose of calculating the flow field, we will, however, set mean lithospheric rotation of the plate motion models used equal to zero by subtracting a constant rotation vector from each plate rotation. In this way, a relative rotation of mean lithosphere and mean mantle is introduced ad hoc.

At first sight, this procedure seems inconsistent. Plate motions are defined relative to hotspots in the models we use, and by setting mean lithospheric rotation to zero in the flow calculation, it is implicitly assumed that the hotspot reference frame represents the no-net-rotation reference frame. However, it is exactly the motion of these hotspots relative to the no-net-rotation reference frame we wish to calculate. The way around this is iteration: from the calculated hotspot motions we can obtain a model of plate motions relative to the no-net-rotation reference frame, which in turn is used to re-calculate hotspot motions. It turns out that after the first iteration step the re-calculated hotspot motions are very similar to the initial results, therefore we will not use any iterations here. The implications of hotspot motion on plate motions and mean lithospheric rotation will be the subject of a separate paper (currently in preparation).

2 THE PLUME MODEL

2.1 The mathematical model

Based on the idea outlined in the Introduction and illustrated in Fig. 2 that an essentially vertical plume conduit is established by a rising plume head and subsequently advected in mantle flow, we will model plume conduits in the following manner.

(1) M (the 'mantle') is a region in space which is bounded by two smooth surfaces (that is, a normal vector can be defined on them everywhere) T (the 'top surface') and B (the 'bottom surface').

(2) A 'plume conduit' is a continuous line within M connecting T and B. Its position and shape depend on time t, thus it can be parametrized as a set of points $\mathbf{x}_\lambda(t)$, $\lambda_B(t) \le \lambda \le \lambda_T(t)$, which we shall call 'conduit elements'.

(3) Two vector fields $\mathbf{v}(\mathbf{x}, t)$ (the 'mantle flow velocity') and $\mathbf{g}(\mathbf{x})$ (the 'gravity field') as well as a scalar field $\eta(\mathbf{x})$ ('viscosity') shall be defined in M (including T and B). T and B as well as $\mathbf{g}$ and η are time-independent, whereas $\mathbf{v}$ may depend on time.

(4) The velocity of each conduit element consists of the ambient mantle flow velocity $\mathbf{v}(\mathbf{x}_\lambda(t), t)$ plus a vertical rising velocity $-\kappa \cdot \mathbf{g}(\mathbf{x}_\lambda(t))/\eta(\mathbf{x}_\lambda(t))$.

(5) λ_B and λ_T are time-dependent, since $\mathbf{v}(\mathbf{x}_\lambda(t), t) - \kappa \cdot \mathbf{g}(\mathbf{x}_\lambda(t))/\eta(\mathbf{x}_\lambda(t))$ will in general not be tangential to B and T.

(6) The point $\mathbf{x}_B$ where the conduit intersects B moves with the component of the mantle flow velocity tangential to B.

(7) The point $\mathbf{x}_T$ where the conduit intersects T is called the 'hotspot'.

2.2 A simple analytical model

To illustrate this model we briefly discuss here a simple 1-D flow that yields hotspot motion in a direction opposite to plate motion. A more extensive discussion of the model is given in Steinberger (1996). We consider a flow field of the form $\mathbf{v}(z, t) = \hat{v}_0(z)\mathbf{v}_s(t)$ in a layer $0 < z < d$ with a surface plate velocity $\mathbf{v}_s(t)$ and a depth-dependent viscosity $\eta(z)$. Any plate-driven flow shall be balanced by a return flow at depth: $\int_0^d \mathbf{v}(z, t)\, dz = 0$. The pressure gradient ∇p that drives the return flow be constant everywhere, and velocity will be zero at depth d.

Let $z(\tilde{t})$ be the depth from which a conduit element rises to the surface according to eq. (5) after a time interval $\tilde{t}$. For all times $\tilde{t}$ greater than the total rising time t_0 from the lower boundary at depth d we set $z(\tilde{t}) = d$. For a conduit starting at the origin, the surface position at time t will then be

$$\mathbf{x}(t) = \int_0^t \mathbf{v}(z(t-t'), t')dt' = \int_0^t \hat{v}_0(z(t-t'))\cdot\mathbf{v}_s(t')dt'\,. \tag{3}$$

If surface plate velocity does not depend on time, this reduces to

$$\mathbf{x}(t) = \mathbf{v}_s \cdot \int_0^t \hat{v}_0(z(t-t'))dt' = \mathbf{v}_s \cdot \int_0^{z(t)} \frac{v_0(z')}{u(z')} dz'\,, \tag{4}$$

where $u(z)$ is the thermal rising speed at depth z. By differentiating we obtain $\dot{\mathbf{x}}(t) = \mathbf{v}(z(t))$, that is the surface velocity of the conduit at a time t after eruption of the plume head is simply the horizontal flow velocity at the depth from which the conduit element rose during time t. A plume will initially move in the direction of plate motion, but in the opposite direction for times corresponding to depths of the return flow. If viscosity is higher, hence rising speed lower, at these depths, the total horizontal displacement during the total rising time t_0 is opposite to the direction of plate motion, and hotspot motion will tend to be opposite to plate motion for longer time periods.

As an example, we consider an upper layer of thickness 300 km and viscosity 2×10^{20} Pa s overlying a lower layer of thickness 600 km and viscosity 2×10^{21} Pa s. If we assume a thermal rising speed of 10.4 cm yr^{-1} in the upper layer (for example corresponding to a plume of radius 45 km and density contrast 60 kg m^{-3}) and a surface motion of 8.6 cm yr^{-1} (Pacific Plate velocity in the vicinity of Hawaii), we obtain a total deflection in the upper layer of about 125 km. This agrees with the estimate of Griffiths & Richards (1989), who determined from the sharpness of the bend in the Hawaiian–Emperor chain that the total deflection of the Hawaiian plume in the uppermost layer is less than about 200 km. In the lower layer, total deflection amounts to about 750 km in a direction opposite to plate motion over a time interval of about 58 Myr. The average rate of hotspot motion during that time is thus about 1.3 cm yr^{-1}, whereas the initial rate (corresponding to flow at the top of the lower layer) is about 1.7 cm yr^{-1}. If instead we take a lower layer of thickness 2100 km and viscosity 10^{23} Pa s, we find an initial rate of surface motion of about 0.6 cm yr^{-1}, which persists over a very long time. In the first case a tilt of 60° is reached after about 100 Myr, leading to possible instability of the conduit, whereas in the second case it

GJI000 21/1/98 16:14:47 3B2 version 5.20
The Charlesworth Group, Huddersfield 01484 517077

takes longer to develop an instability, according to the estimate that will be given in Section 2.4. A more general discussion of results is given in Steinberger (1996).

The example demonstrates that for reasonable model parameters a deflection rate of the order 1 cm yr^{-1} over a timespan approaching the observed lifetime of plumes $>\sim 100$ Myr is possible. Thus a more accurate numerical investigation is justified and will be presented below. Since return flow on a sphere is by its nature 3-D, this will give more meaningful results.

2.3 The numerical model

Based on the mathematical model, the following numerical model is used.

The mantle

The mantle M is a spherical shell. The bottom surface B is a sphere of radius $r_B = 3571$ km, 100 km above the core–mantle boundary, and the top surface T is a sphere of radius $r_T = 6271$ km, at a depth 100 km. This top surface is chosen because melting occurs around that depth, and magma rises more or less vertically through cracks in the brittle lithosphere, which comprises approximately the top 100 km of the Earth. The choice of B is consistent with the assumption that the bottom 100 km of the mantle is a thermal boundary layer of low viscosity which feeds the plume, and the conduit starts at the top of this boundary layer. Values chosen for r_T and r_B do not significantly affect the results.

The plume conduit, initial condition

The plume conduit consists at time t of a set of $n(t)$ conduit elements at the positions $\mathbf{x}_i(t)$ [radial coordinate $r_i(t)$], $i = 1 \ldots n(t)$. The initial condition is a vertical conduit at time t_h ('eruption of the plume head') with $n(t_h)$ approximately equally spaced conduit elements. The first conduit element is on B.

Mantle flow velocity, gravity field, viscosity

(1) The ambient mantle flow velocity is first calculated on a grid using the method of Hager & O'Connell (1979, 1981) (see Appendix A). Typically, we choose a grid with 16×32 points on each layer and 15 radial layers. Velocity at the positions of the conduit elements is interpolated from values on $4 \times 4 \times 2$ grid-points, which surround the position of the conduit element. Two 2-D polynomial interpolations on horizontal 4×4-grids are carried out (Press *et al.* 1989). Radial interpolation is carried out linearly because the mantle flow field does not vary smoothly in the radial direction, owing to discontinuities in the viscosity structure. It is implicitly assumed that the presence of the conduit does not alter the ambient flow field. This is probably approximately true, due to the small size of the conduit.

(2) Gravity is in the radial direction and has constant magnitude. This is approximately true in the Earth's mantle.

(3) The mantle consists of spherical shells, within each of which the viscosity is constant.

Vertical rising; total velocity of conduit elements

The velocity of each conduit element consists of the ambient flow velocity $\mathbf{v}(\mathbf{x}_i(t), t)$ plus a vertical rising velocity. The rising speed should be given approximately by

$$u_i = u_0 \cdot \frac{\eta_0}{\eta} = \frac{k_c \Delta\rho g r_c^2}{\eta}\,, \tag{5}$$

where $\Delta\rho$ is the density contrast between the plume and its surroundings, g is gravity, r_c is the conduit radius, k_c is a numerical constant, η is the viscosity of the surrounding mantle and η_0 is the normalizing viscosity. For a chemical plume, Richards & Griffiths (1988) determined experimentally $k_c \approx 0.54$. If we choose $\eta_0 = 10^{21}$ Pa s and assume $\Delta\rho = 60$ kg m^{-3} (which would correspond to a temperature contrast of approximately 400 K for a thermal plume), and $r_c = 45$ km, we obtain $u_0 \approx 2.1$ cm yr^{-1}. It should, however, be larger for a thermal plume. Owing to conduction, the temperature of the mantle surrounding the conduit will increase, thus its viscosity will decrease, and therefore the conduit (which, in this case, will lose its well-defined identity) will rise faster. In this case, it is required that the flow of material *through* the conduit (which may be much faster than the buoyant rising velocity of the conduit) is sufficiently vigorous in order to replace heat lost through conduction. In all calculations shown here we will choose $u_0 = 2.2$ cm yr^{-1} for $\eta_0 = 10^{21}$ Pa s.

Time integration

The trajectory of a conduit element is determined by the differential equation

$$\frac{d\mathbf{x}_i}{dt} = \mathbf{v}(\mathbf{x}_i(t), t) + u_0 \frac{\eta_0}{\eta(r_i(t))}\mathbf{e}_r =: \mathbf{v}_c(\mathbf{x}_i(t), t)\,, \tag{6}$$

where $\mathbf{e}_r$ is the radial unit vector, which we integrate with the Euler method,

$$\mathbf{x}_i(t + \Delta t) = \mathbf{x}_i(t) + \mathbf{v}_c(\mathbf{x}_i(t), t) \cdot \Delta t\,, \tag{7}$$

where Δt is the stepsize. Normally we will choose $\Delta t = 0.2$ Myr. The radial coordinate of the first conduit element will be reset to r_B after each integration step. This ensures that the conduit stays connected with B.

Creating and removing conduit elements

Conduit elements disappear if they cross T. If the distance $\|\mathbf{x}_{i+1} - \mathbf{x}_i\|$ between neighbouring conduit elements becomes larger than d_{max} (usually 55.5 km), a new conduit element is created at the mid-point $(\mathbf{x}_{i+1} + \mathbf{x}_i)/2$ and the indices are changed accordingly.

Crossing boundaries

At a boundary with discontinuously varying viscosity, $\mathbf{v}_c(\mathbf{x}_i(t), t)$ will also be discontinuous. If such a boundary is crossed during the integration step (7), the time and position of the crossing is calculated by linear interpolation, and the next integration step is started from there. It occasionally happens that in this way an integration step starts at a boundary point

GJI000 21/1/98 16:15:28 3B2 version 5.20
The Charlesworth Group, Huddersfield 01484 517077

x, where

$$\lim_{\epsilon\to 0} v_{c,r}(\mathbf{x}-\epsilon\mathbf{e}_r, t) > 0 \quad \text{and} \quad \lim_{\epsilon\to 0} v_{c,r}(\mathbf{x}+\epsilon\mathbf{e}_r, t) < 0 \quad \text{for} \quad \epsilon > 0, \tag{8}$$

that is the value of $\mathbf{v}_c$ just above the boundary has a downward component and the value of $\mathbf{v}_c$ just below the boundary has an upward component. In this case, the radial velocity component $v_{c,r}(\mathbf{x}, t)$ is set equal to zero. In any other case the viscosity value at the other side of the boundary is used for the next step.

Because of the discontinuities of $d\mathbf{x}_i/dt$, the more sophisticated Runge–Kutta method with adaptive stepsize control does not bring about any improvement in terms of accuracy or speed of calculation.

2.4 Tilting, break-up and extinction of plume conduits

It is an important model constraint that plume conduits be stable for times equal to the observed ages of hotspots in the places where actual hotspots are observed.

2.4.1 Tilting of plume conduit without break-up?

As was noted in the Introduction, it is expected that the shape of a conduit becomes unstable once it is tilted more than about 60° from the vertical. However, this instability requires some time to develop into a complete break-up of the conduit into separate drops. For a sufficiently high viscosity of the surrounding mantle the time required should be longer than the observed lifetime of plumes, which is approximately $t_l = 100$ Myr: from the geometry of the problem one can conclude that the time required between the instability occurring and a break-up should be at least as long as the time required for a conduit element to rise buoyantly by one conduit diameter. According to eq. (5), this time is larger than t_l if

$$\eta > 0.5 k_c \Delta\rho g r_c t_l . \tag{9}$$

If we use the same numerical values as previously we obtain $\eta > 2.3\times 10^{22}$ Pa s.

2.4.2 Break-up of plume conduit without extinction of hotspot?

If a conduit breaks up into separate drops, it would mean almost certain extinction of the hotspot, unless the thermal rising velocity is high enough at that point. This is shown by the following scaling argument: consider a plume conduit of radius r and length l, with a temperature difference of ΔT relative to the surroundings. Solving the diffusion equation for cylindrical symmetry and stationary conditions without heat generation gives a rate of heat loss through conduction of $P_1 = \Delta T 2\pi l k$, where k is thermal conductivity. On the other hand, the rate at which additional energy gets advected through the conduit is $P_2 = r^2 \pi v_c \Delta T \rho C$, where C is heat capacity, ρ is density and v_c is the upward speed of the material inside the conduit. If the conduit should survive, we require $P_2 > \sim P_1$, therefore

$$v_c > \sim \frac{2l\kappa}{r^2} , \tag{10}$$

where $\kappa = k/(\rho C)$ is diffusivity. Incidentally, this equation gives (independent of r) a lower limit for the material flux through the conduit of $2l\kappa \approx 7.2$ m^3 s$^{-1} \approx 0.2$ km^3 yr^{-1} for plumes rising from the CMB. For $\Delta\rho = 60$ kg m^{-3} this would correspond to an anomalous mass flux of about 0.4×10^3 kg s^{-1}, only a little higher than the lower limit of observed plume buoyancy fluxes (Davies 1988; Sleep 1990).

If the conduit gets tilted too strongly and it breaks up into drops, the buoyant rising velocity of the drops in that layer should be at least as large as v_c, so that the flow through the conduit can continue. If we assume the drops rise with the same speed as the conduit (which will not be exactly the case, due to the change in shape), we obtain from (10) and (5)

$$\eta < \frac{k_c g r^4 \Delta\rho}{2\kappa l} . \tag{11}$$

Reasonable numbers for the Earth are $\kappa = 1.2\times 10^{-6}$ m^2 s^{-1}, $l = 2800$ km, $\Delta\rho = 60$ kg m^{-3} and $r = 50$ km, which gives $\eta < 3.0\times 10^{20}$ Pa s, and even smaller values for smaller radii.

According to the two estimates above we will consider in some of the numerical calculations that follow that a hotspot becomes 'extinct' if its conduit gets tilted more than 60° in

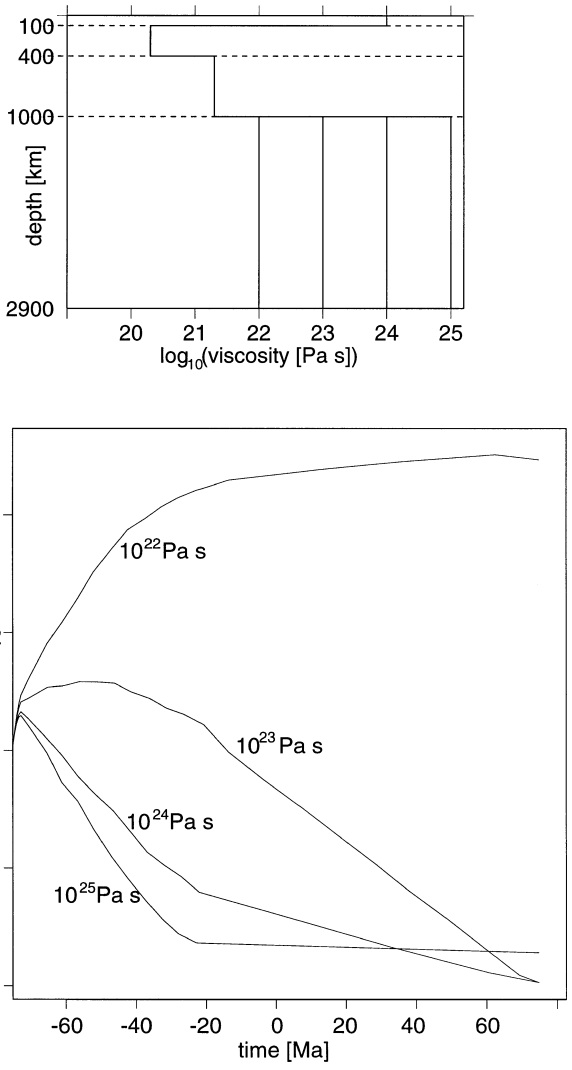

Figure 4. E–W motion of a hotspot calculated for the viscosity structures shown, kinematic flow only and constant present-day plate velocity. Eruption of plume head at 75 Ma at 160°W, 20°N. Respective viscosities below a depth of 1000 km are indicated.

GJI000 21/1/98 16:15:52 3B2 version 5.20
The Charlesworth Group, Huddersfield 01484 517077

a mantle layer with a viscosity between 3.0×10^{20} and 2.3×10^{22} Pa s.

3 NUMERICAL RESULTS OF HOTSPOT MOTION, TILTING OF PLUME CONDUITS AND GLOBAL DISTRIBUTION OF HOTSPOTS

3.1 Hotspot motion for time-independent kinematic flow

In Section 2.2 the effect of flow driven by surface plate motions was discussed for an idealized setting, and here we shall present results for actual plate geometries and velocities. Fig. 4 shows the motion of a hotspot roughly at the present position of Hawaii, for constant kinematic flow. Although the mantle flow field is now neither exactly horizontal nor parallel to plate motion, the curves still largely represent a vertical profile of horizontal mantle flow velocity, as explained in Section 2.2. In most of the curves, kinks are evident about 3 Myr after the eruption of the plume head (corresponding to conduit elements rising 11 cm yr^{-1} between 400 and 100 km depth), and again about 55 Myr later (corresponding to conduit elements rising 1.1 cm yr^{-1} between 400 and 1000 km depth). The figure shows that even for a very high viscosity in the lower mantle (10^{23} Pa s) most of the plate-driven return flow takes place in the lower mantle, and will therefore lead to advection with a substantial speed over long times.

3.2 Hotspot motion for time-dependent kinematic flow

We will now introduce a change in plate velocity. Fig. 5 shows how hotspot motion depends on the time interval between eruption of the plume head and change in plate velocity. We choose an initial location at the present position of the Hawaiian hotspot. In reality, a rather abrupt change in Pacific Plate velocity similar to that shown here occurred at about 43 Ma. As long as plate motion does not change, the hotspot gets advected initially in the direction of plate motion, but the direction reverses, consistent with Fig. 4. If a change in plate velocity occurs while or after the direction reverses, the hotspot

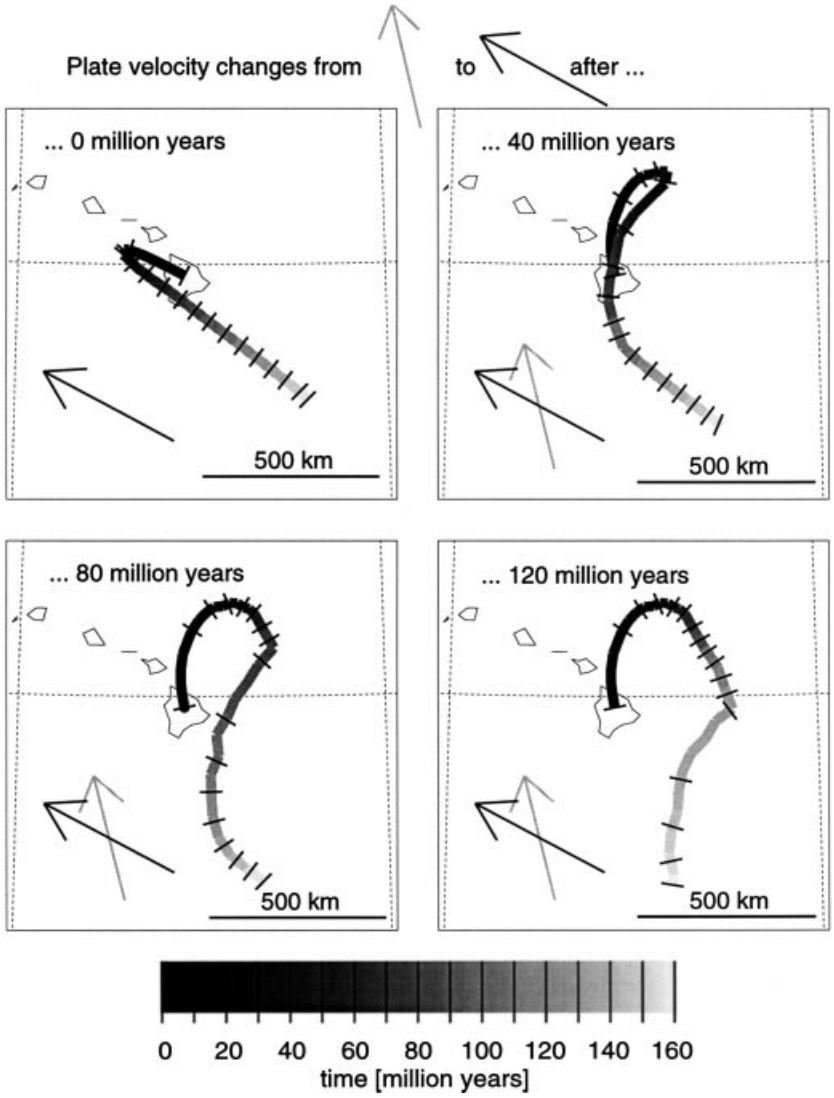

Figure 5. Hotspot motion calculated for the viscosity structure in Fig. 4 with 10^{23} Pa s below depth 1000 km and kinematic flow only. Eruption of plume head at time zero.

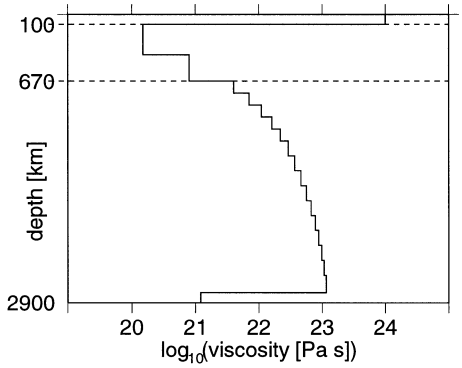

Figure 6. Preferred viscosity structure.

gets advected in the direction of new plate motion minus old plate motion during a transient period. Afterwards, hotspot motion is opposite to the new plate motion.

3.3 The preferred model: results for initial positions on a grid with equal eruption times

3.3.1 Motion and tracks of hotspots

The situation may change considerably when flow driven by internal density heterogeneities is added. We first present results for a model that has a low viscosity in the upper mantle and a very high viscosity in the lower mantle (Fig. 6). Fig. 7 shows a rather small relative motion between hotspots

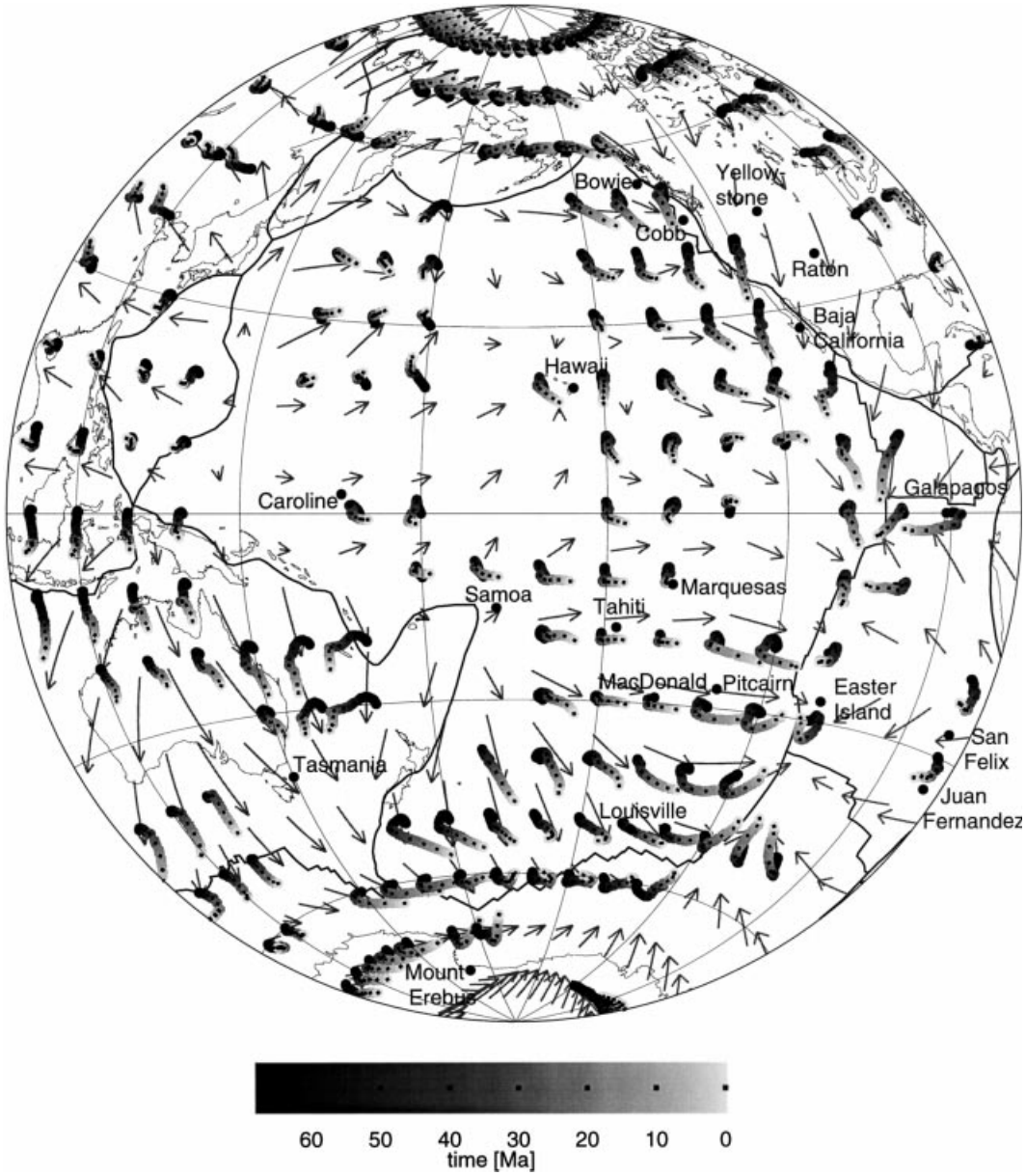

Figure 7. Hotspot motion calculated for our preferred viscosity structure and a conversion factor $(\delta\rho/\rho)/(\delta v/v)=0.2$, time-dependent plate motions and advection of density heterogeneities. Eruption of plume head 68 Myr ago at initial positions on a grid. Only shown are hotspots that have not become extinct at present. Actual hotspots are shown as black dots. Arrows indicate present-day flow at a depth of 670 km, with lengths equal to the total displacement that would result from 68 Myr of constant flow.

GJI000 21/1/98 16:16:14 3B2 version 5.20
The Charlesworth Group, Huddersfield 01484 517077

approximately at the positions of several actual Pacific hotspots with well-determined hotspot tracks (Hawaiian, Louisville, Kodiak-Bowie), and a coherent motion in the no-net-rotation reference frame; African hotspots (Fig. 8), on the other hand, show no obvious coherent motion. In this model, for many hotspots the direction and magnitude of motion are similar to flow at the top of the lower mantle.

Fig. 9 shows the tracks relative to the Pacific Plate for the same case. The bend in the Hawaiian–Emperor chain is about as sharp as observed; the radius of curvature of the bend is a measure of plume deflection in the uppermost mantle layer, which in turn depends on the viscosity there, as pointed out by Griffiths & Richards (1989). Here Pacific Plate motion has been adjusted to account for the coherent component of hotspot motion (Fig. 7), as will be discussed in more detail in a forthcoming paper.

3.3.2 Hotspot distribution and tilting of plume conduits in mantle flow

Over-tilting due to kinematic flow can be avoided by a low enough viscosity in the asthenosphere and high enough viscosity below. A low viscosity in the asthenosphere ensures a high buoyant rising velocity such that conduits do not get strongly tilted. A sufficiently high viscosity below the asthenosphere results in a sufficiently small deflection due to return flow (see Fig. 3).

Figs 7 and 8 show that, for that reason, in our preferred model a large fraction of plumes survive for 68 Myr. There are plumes surviving close to all the sites of actual hotspots on the Pacific Plate. The areas where plumes cannot survive for 68 Myr in this model are in many cases areas overlying a dense lower mantle, which roughly agrees with areas of past and

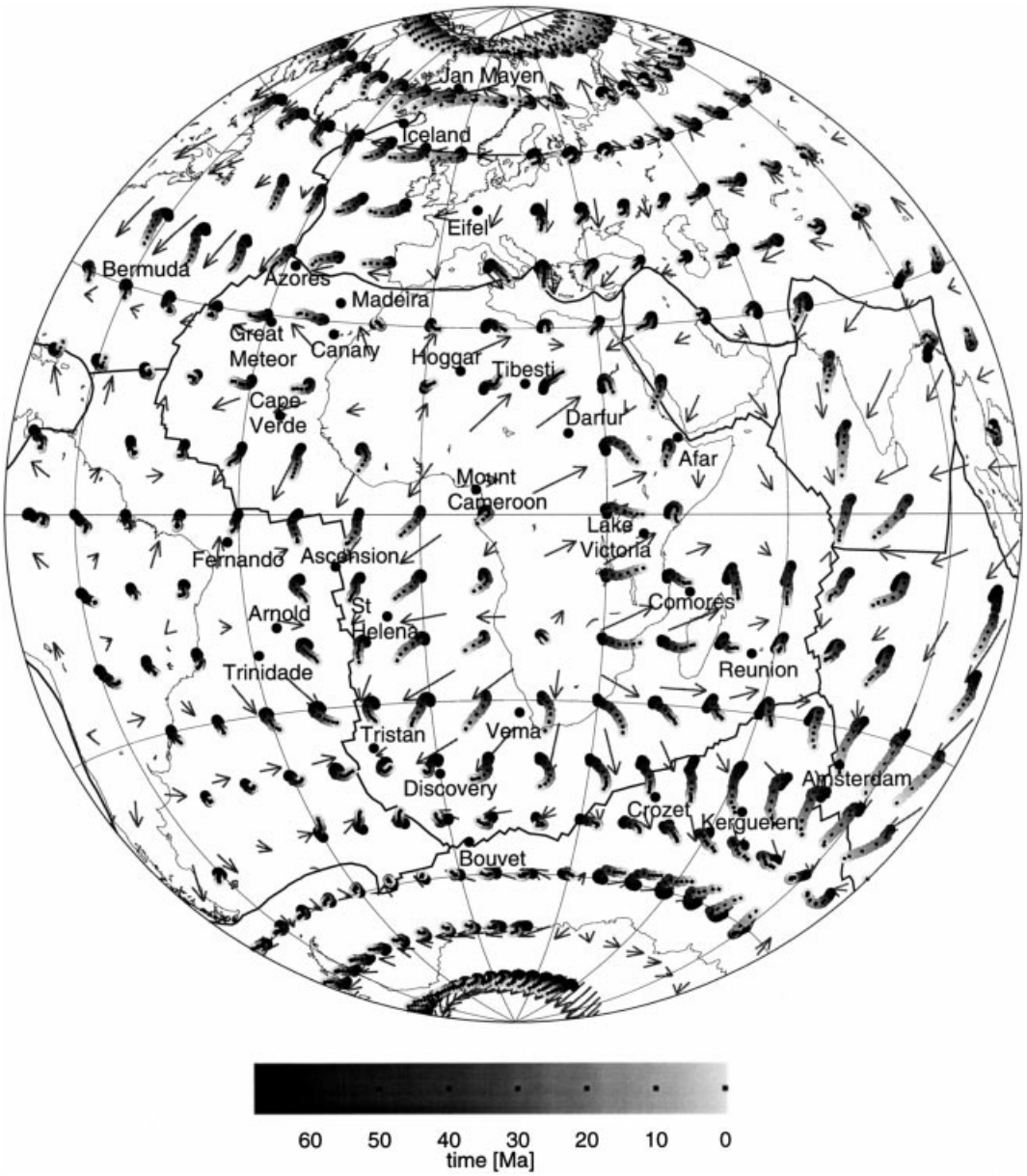

Figure 8. Results for the opposite hemisphere; see Fig. 7.

GJI000 21/1/98 16:16:25 3B2 version 5.20
The Charlesworth Group, Huddersfield 01484 517077

Figure 9. Calculated hotspot tracks on the Pacific Plate for the same model as in Fig. 7. Other details as in Fig. 1.

present subduction, and therefore areas of large-scale downwellings which cause a strong deformation of plume conduits in the mid-mantle. This resembles the actual distribution of hotspots—they tend not to be located in these areas. Fig. 10 shows that only about 11 out of 47 hotspots are located over positive seismic anomalies averaged over the lower mantle, and only three hotspots are located in regions where subduction took place during the past 100 Myr (Tasmania, Yellowstone, Raton/New Mexico). There are only three actual hotspots in Figs 7 and 8 that are further than 10° from any calculated hotspot: Yellowstone, Raton/New Mexico and Eifel. However, the Yellowstone hotspot may be younger than 68 Ma, as the eruption of the Yellowstone plume head has been associated with the Columbia River Basalts (age ~16 Ma). Therefore, its existence does not contradict this model. Raton and Eifel might not be hotspots at all (Richards *et al.* 1988; Sleep 1990); instead, they might be related to intraplate rifting in the Rio Grande Rift and Rhine Graben.

Figs 7 and 8 also show that, in the vicinity of ridges, hotspots tend to get advected towards the ridge, owing to the kinematic return flow. This might help to explain the fact that observed hotspots also tend to be frequently at or near ridges.

To further illustrate the tilting of plume conduits, Figs 11, 12 and 13 show the calculated present-day shape of some plume conduits. The source regions of plumes near the core–mantle boundary tend to be advected with the deep-mantle horizontal flow towards large-scale upwellings and therefore concentrate in regions of 'hot', that is seismically slow, lower mantle. There

GJI000 21/1/98 16:16:27 3B2 version 5.20
The Charlesworth Group, Huddersfield 01484 517077

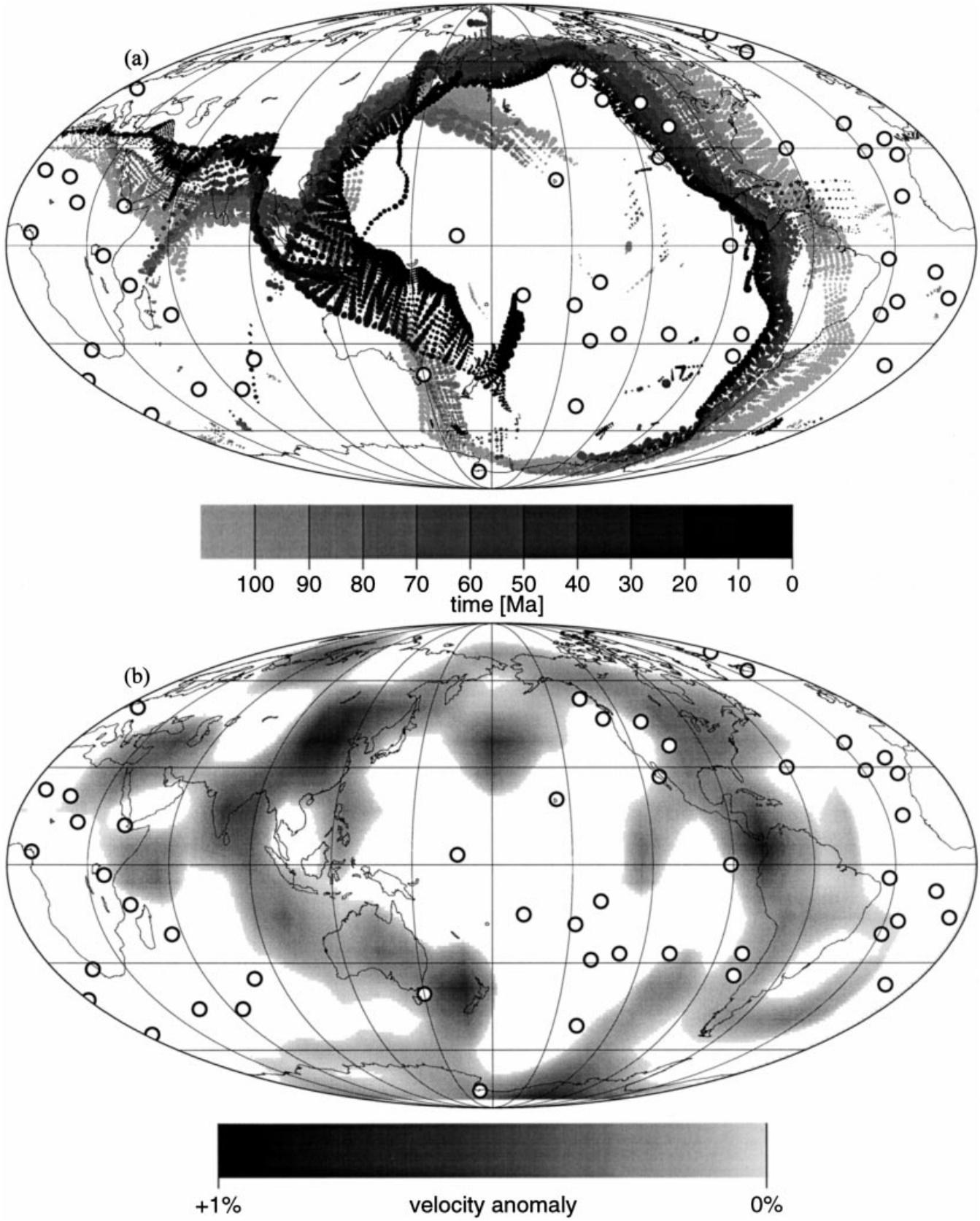

Figure 10. (a) Subduction during the past 119 Myr. Locations and amounts of subduction are calculated from past plate motions and plate geometries. Between 0 and 64 Ma we use the data of Gordon & Jurdy (1986); before that we use the data of Lithgow-Bertelloni (1994). Boundary locations were interpolated at 2 Myr intervals. Area of dots corresponds to amount of subducted material; however, overlap between dots occurs. (b) Depth average of seismic velocity anomalies in the lower mantle from the model SH12/WM13 of Su *et al.* (1994). Present actual hotspot locations are shown as a white dot surrounded by a black circle.

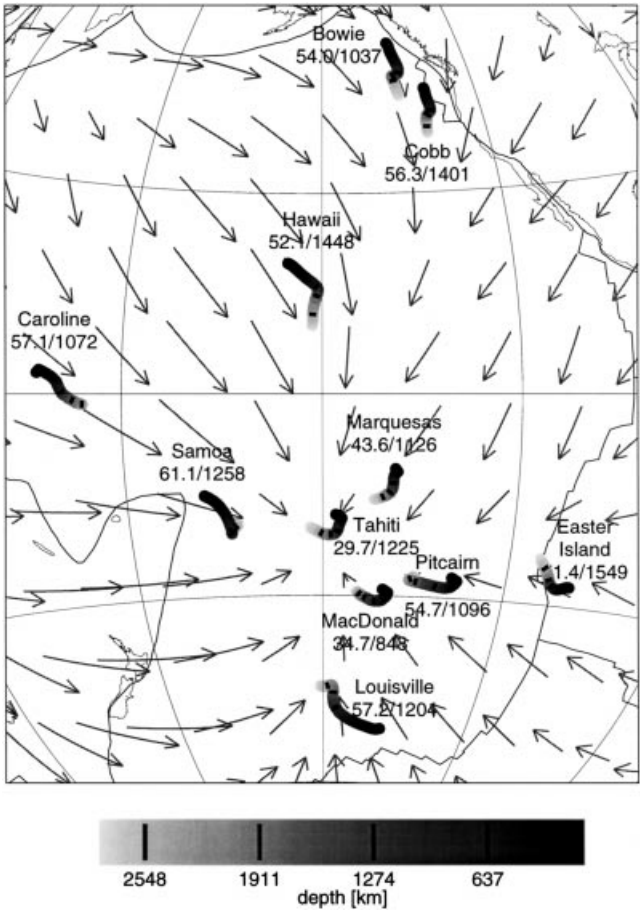

Figure 11. Calculated present-day shapes of plume conduits in the Pacific for the same model as in Fig. 7. Numbers indicate the maximum tilt in mantle layers with viscosity between 3×10^{20} and 2.3×10^{22} Pa s, and the depth from which a conduit element rises to the surface during the time of calculation (68 Myr). Tick-mark depth intervals are 0.1 Earth radii. Arrows indicate present-day flow at depth 2700 km, with lengths equal to the total displacement that would result from 68 Myr of constant flow.

are possibly interesting geochemical implications in cases where the calculated positions at the core–mantle boundary are very close, such as for Reunion and Kerguelen. Hotspot surface motion, however, is more closely related to horizontal flow in the upper part of the lower mantle; mantle flow below depths from which conduit elements may rise to the surface as indicated in Figs 11 and 13 has no influence on hotspot surface motion.

Despite a strong viscosity increase with depth, horizontal flow speed just above D″ has on average similar *magnitude* as in the top part of the lower mantle (compare Figs 7 and 8 with Figs 11 and 13; see Fig. A2)—internal density heterogeneities tend to be comparatively strong in the lowermost mantle (Su, Woodward & Dziewonski 1994). Therefore, in many cases, such as for Hawaii, motion at the base of the conduits (from the initial plume locations that can be inferred approximately from Figs 7 and 8 towards the present locations in Figs 11 and 13) is larger than the observed surface hotspot motion. Moreover, relative motion of hotspots on the Pacific Plate is even smaller (Fig. 7). This is partly due to coherence of the flow associated with plate motion; it might also be partly coincidence. This result can help to reconcile the observation that apparently stationary plumes originate from a convecting lower mantle.

Horizontal flow *directions* in the upper and lower parts of the lower mantle are often rather different though, resulting in significant tilt of the plume conduits. Maximum tilts in the mid-mantle, where they may lead to extinction of the hotspot, are also indicated in Figs 11 and 13. Of course, numbers for both depth and tilt angle in these figures will depend on the assumed age of the plume, and in general increase with age.

3.4 Results for random initial positions and eruption times

3.4.1 The numerical experiment: motivation, implementation and results

It may be suspected that a correlation of hotspot distribution with seismic tomography is not due to the fact that plumes primarily originate in seismic tomographic 'hot' regions, but rather might be due to the advection of plumes into large-scale upwellings and to a longer lifetime of plumes in these regions, both of which we observed in the calculations for our preferred model. In this section, which was motivated by a paper by Jurdy & Stefanick (1990), we specifically address this question by performing the following numerical experiment.

We start off with vertical conduits left behind by plume heads erupted at randomly chosen positions and times between

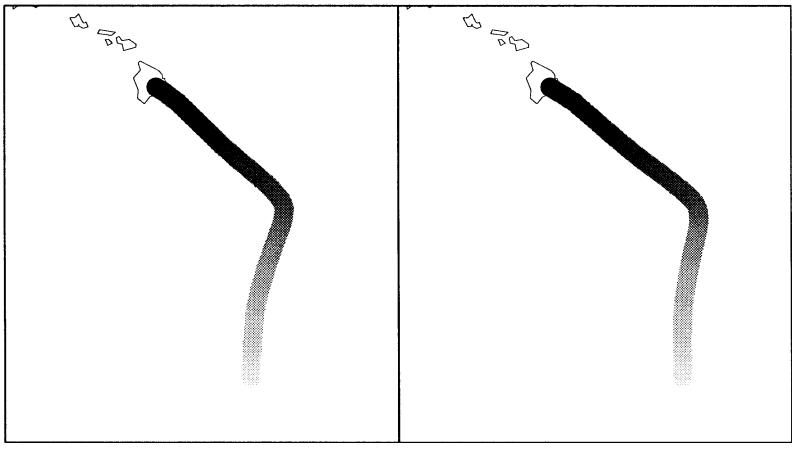

Figure 12. Stereogram of the calculated present-day shape of the Hawaiian plume conduit. Calculation for the same model as in Fig. 7.

GJI000 21/1/98 16:16:32 3B2 version 5.20
The Charlesworth Group, Huddersfield 01484 517077

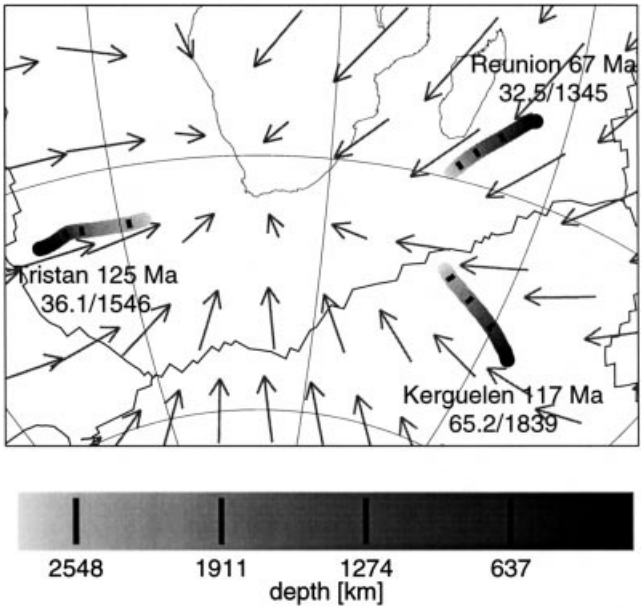

Figure 13. Calculated present-day shapes of Tristan, Reunion and Kerguelen plume conduits for the same model as in Fig. 7. Eruption time of plumes is indicated, mantle density heterogeneities are advected for 68 Ma only. Other numbers and arrows as in Fig. 11.

0 and 150 Ma. The conduits are subsequently advected in large-scale mantle flow up to extinction or the present time, whichever comes first.

Fig. 14 shows the calculated present hotspot locations. As in Figs 7 and 8 the distribution is similar to what is observed: hotspots cluster in certain areas of large-scale upwellings, especially close to ridges and above regions with a hot lower mantle (for example in the central Pacific, $\approx 150°$W, 15°S), and they are less frequent in regions of large-scale downwellings, especially areas of present and past subduction such as under central and western North America. Both effects are more pronounced if only plumes above a certain age (shown in darker shades) are considered, for the obvious reason that they had more time to migrate or to become extinct.

3.4.2 *Statistical analysis of results*

A total of 701 out of an initial 1000 plumes survive until the present in this experiment. The number of surviving plumes in bins of 15 Myr is plotted versus age (at the centre of the bin) in Fig. 15. Apart from statistical fluctuations, we observe an approximately linear decrease of the number of plumes with age. After about 100 Myr, only about half of the original number has survived. This agrees well with the observed lifetime of plumes.

In order to address the question whether the observed distribution of hotspots can be fully explained (in a statistical sense) by advection and different lifetimes in different regions, we determine the correlation of the calculated surface hotspot

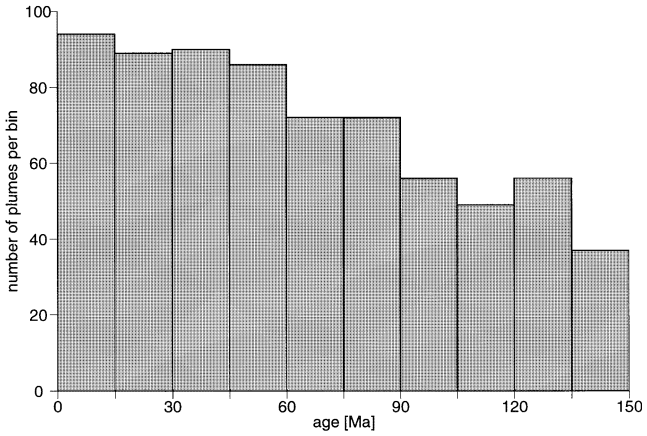

Figure 15. Histogram showing the number of surviving plumes in bins of 15 Myr plotted versus age for the plume distribution shown in Fig. 14.

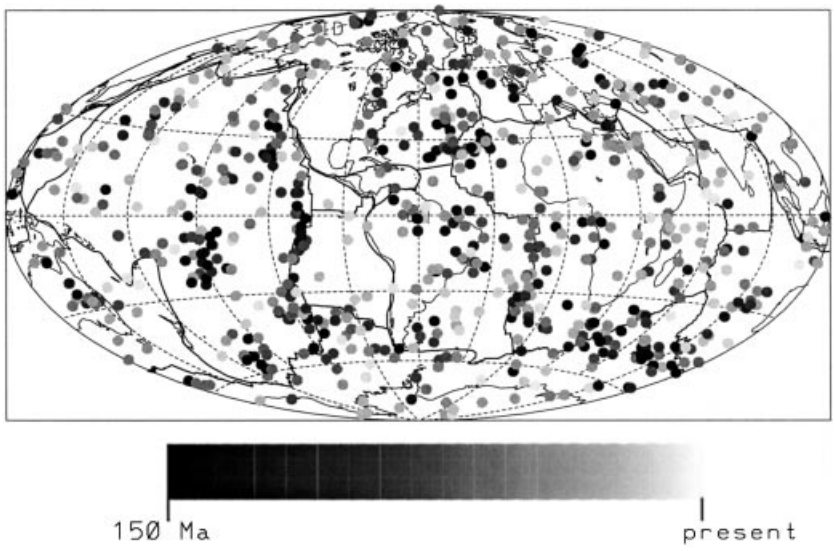

Figure 14. Calculated present positions of hotspots for random locations and times of eruption between 0 and 150 Ma, otherwise same model as in Fig. 7. Only those hotspots for which the conduits have not been tilted more than 60° in mantle layers with viscosity between 3×10^{20} and 2.3×10^{22} Pa s are plotted. Hotspot age is indicated by shade.

GJI000 21/1/98 16:16:43 3B2 version 5.20
The Charlesworth Group, Huddersfield 01484 517077

positions with seismic velocity anomalies at various depth levels. The results are compared with the correlation of the actual hotspot distribution and the tomographic models (Fig. 16).

Both curves for actual and calculated plume distributions look similar—both have minima in the lower part of the lower mantle and close to the top of the lower mantle, and values close to zero in between. However, the first minimum is deeper for the observed distribution and the second minimum is deeper for the calculated one. The negative correlation with upper-mantle seismic anomalies represents a concentration of calculated hotspot locations above a hot upper mantle, corresponding to the clustering of hotspots near ridges shown in Fig. 14.

The correlation with the initial random distribution (shown as a dotted line) is on average much closer to zero, thus the differences of the calculated plume distribution from a random set of points are statistically significant.

3.5 Results for other models

3.5.1 Model 2, showing that a low viscosity in the upper mantle is required below the Pacific

Fig. 17 shows the result for a relatively high viscosity in the upper mantle. The initial location of the plume is chosen such that the present location is at Hawaii. The calculated track on the Pacific Plate does not have the sharp bend observed in the Hawaiian–Emperor chain. This happens because the plume deflection in the uppermost mantle, hence the radius of curvature of the bend, is very large for a viscosity of 10^{21} Pa s in this layer. However, since there are no sharp bends in hotspot tracks on the African Plate, we cannot use this constraint on upper-mantle viscosity there.

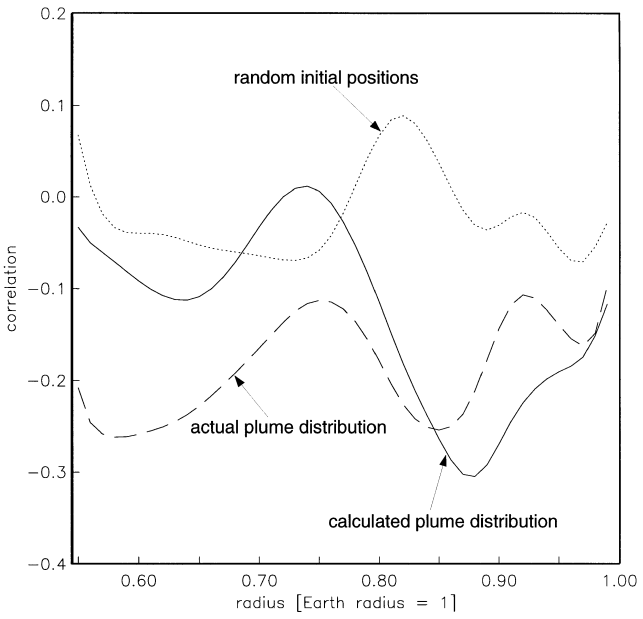

Figure 16. Correlation of actual and calculated (Fig. 15) plume distributions with tomographic model SH12/WM13 (Su *et al.* 1994) as a function of depth. The correlation of the random initial distribution is shown for comparison. Plume distribution and tomographic model are expanded in spherical harmonics, and eq. (5) of O'Connell (1971) is used.

Fig. 18 shows yet another problem with an upper mantle with a canonical viscosity value 10^{21} Pa s under the Pacific. In this case the flow associated with the fast-moving Pacific, Nazca and Cocos plates overtilts plume conduits and, for this calculation, not a single conduit in the entire Pacific Ocean survives for 68 Myr. Unless for some reason the buoyant rising speed of a conduit is significantly higher than assumed, a considerably lower viscosity in the upper mantle below the Pacific can be concluded.

3.5.2 Model 3, showing that a high viscosity in the lower mantle is required

In Fig. 19, the hotspot motion for a higher conversion factor and somewhat lower viscosity in the lower mantle is shown for initial hotspot locations on a 10° grid in the Pacific region. In this calculation the relative motion of hotspots is far too large (5–10 cm yr^{-1}) to be compatible with the observed slow relative motion of hotspots on the Pacific Plate. This faster relative motion is caused by a stronger flow field in the lower mantle that is not in a coherent direction over the whole plate. We therefore conclude that the viscosity in the lower mantle has to be higher and flow velocities smaller than in this example. Features of this model are discussed in more detail by Steinberger (1996).

3.5.3 Model 4: what happens for an even lower viscosity in the asthenosphere?

Fig. 20 shows calculated hotspot motion for the case of an even lower upper-mantle viscosity as proposed by Hager (1991), an earlier eruption time and larger density anomalies.

In this case, most of the hotspot motion represents flow in the lower mantle, since the conduit elements will rise buoyantly from 670 km depth to the base of the lithosphere in only a few million years, and hence are not deflected by much in the upper mantle. Because of the very low viscosity in the upper mantle, plate motions are not strongly coupled to flow in the lower mantle, therefore there is less coherent motion under one plate. Besides the larger density anomalies, the essentially free upper boundary of the lower mantle is another reason that convection in the lower mantle is more vigorous than in the preferred model. Flow out of the large upwellings in the lower mantle is concentrated in the upper mantle, where plumes are not deflected appreciably. Therefore, the advection of plumes is almost entirely towards upwellings: conduits move towards the locations of several actual hotspots (Hawaii, Bowie Seamount, Caroline Islands and Samoa, Pitcairn Island), but they do not stay there. They all converge on a location close to the Tahiti hotspot, with other hotspots close by; this is the location of the predominant upwelling from the lower mantle.

This raises another possibility: plumes might be stationary where they are, not because flow in the lower mantle is so slow, but because they have already been advected into large-scale stationary upwellings in the lower mantle, which have not yet been resolved by seismic tomography. Higher-resolution seismic tomographic results for the lower mantle may reveal whether there are sources of large-scale upwellings beneath hotspots. Results are similar, but less dramatic if a conversion factor of 0.2 and an eruption time of 68 Ma are assumed (Steinberger 1996).

GJI000 21/1/98 16:16:54 3B2 version 5.20
The Charlesworth Group, Huddersfield 01484 517077

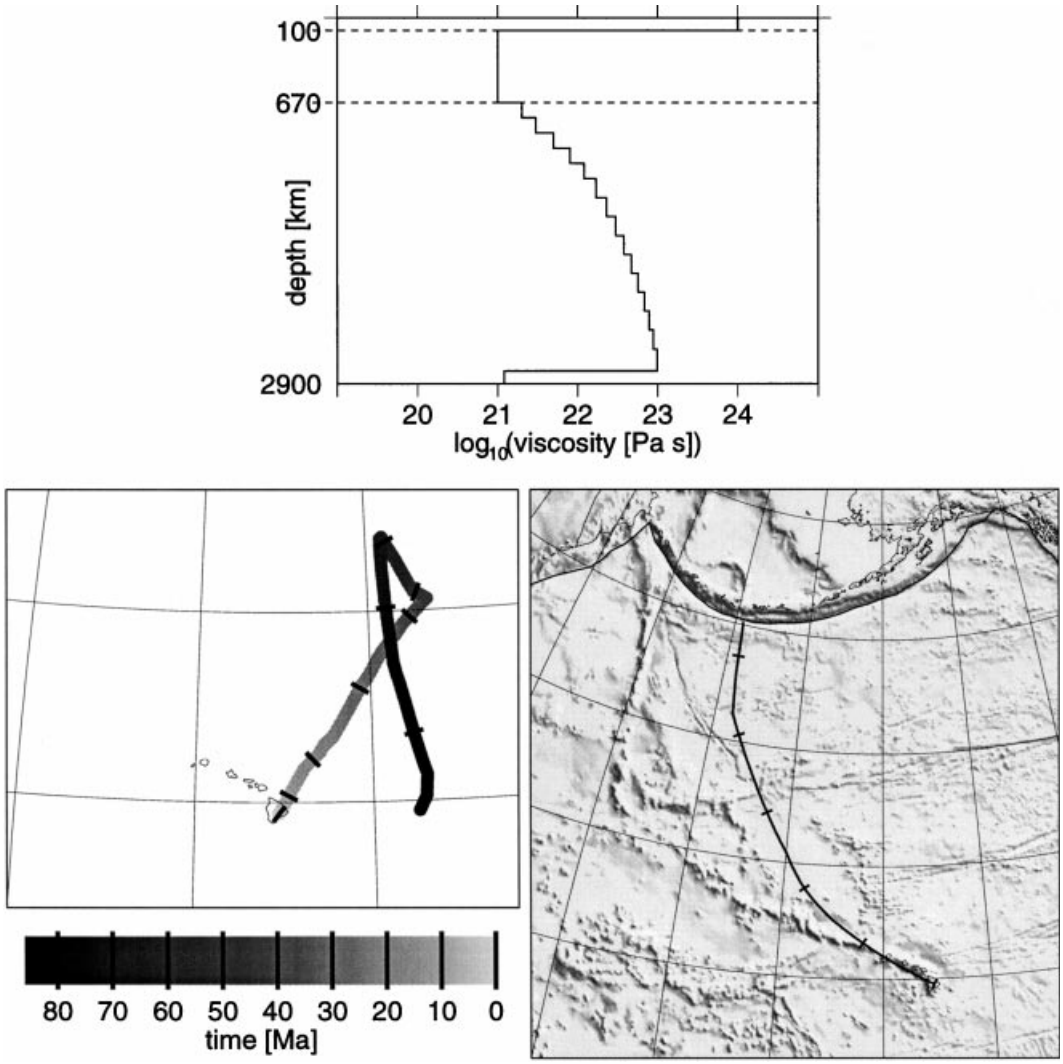

Figure 17. Calculated motion of Hawaiian hotspot (left) and corresponding track on the Pacific Plate for a conversion factor $(\delta\rho/\rho)/(\delta v/v)=0.2$ and the viscosity structure shown, time-dependent plate velocities and advection of density heterogeneities. Eruption of plume head at 86 Ma.

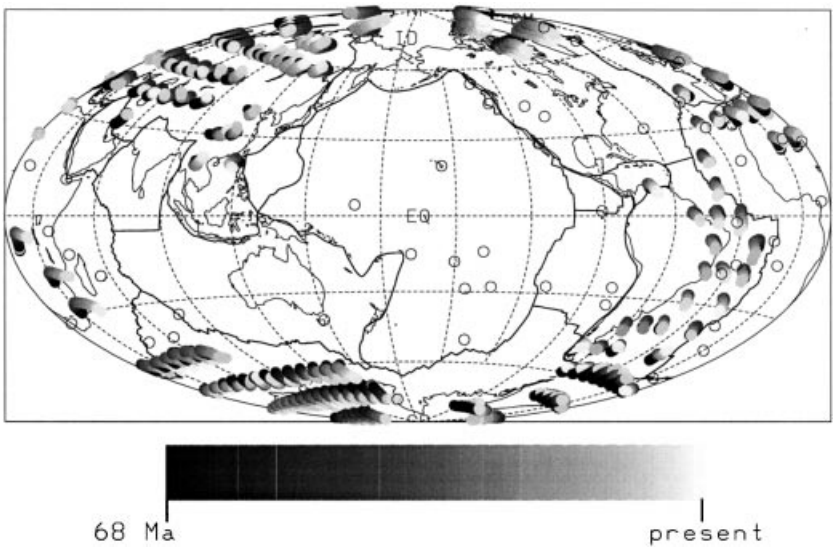

Figure 18. Calculated hotspot motion for eruption of plume head at 68 Ma at initial positions on a grid, otherwise the same case as in Fig. 17. Only shown are hotspots that have not become extinct at present. Actual hotspot locations are shown as circles for comparison.

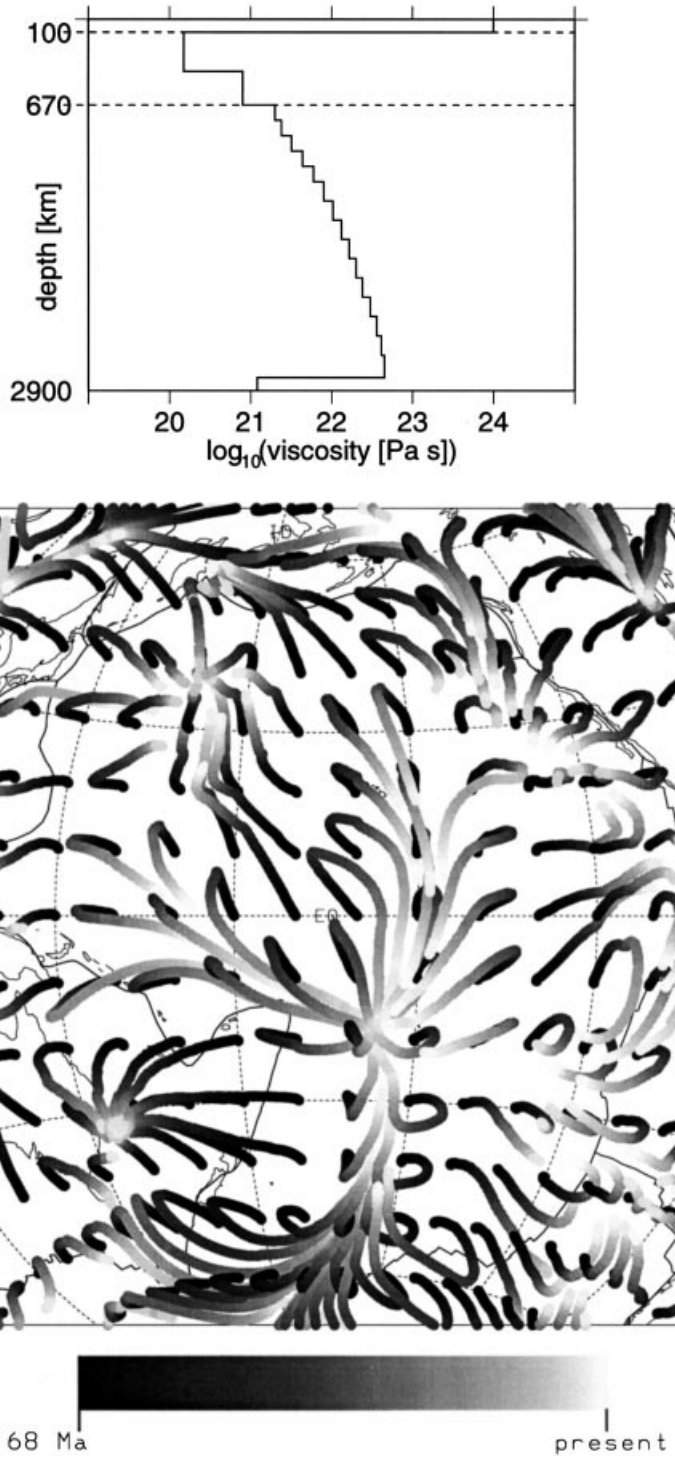

Figure 19. Hotspot motion calculated for a conversion factor $(\delta\rho/\rho)/(\delta v/v)=0.4$ and the viscosity structure shown, time-dependent plate motions and no advection of density heterogeneities. Eruption of plume head at 68 Ma at initial positions on a grid.

4 CONCLUSIONS, DISCUSSION AND OUTLOOK

The primary motivation for this work was to improve our understanding of the hotspot reference frame. We began with the apparent paradox that several hotspots under one plate seem to be fixed relative to each other, in spite of the fact that plates move on the surface and we would therefore expect equally rapid convective motion inside the Earth. Starting from this observation, we discussed constraints on Earth structures which are compatible with the observed apparent fixity of hotspots. We also discussed a possible coherent motion of hotspots under one plate, due to a plate-driven return flow. We began by considering simple 1-D models with a plate on top and a return flow at depth. This led to the conclusion that for certain earth models a coherent motion of

GJI000 21/1/98 16:17:08 3B2 version 5.20
The Charlesworth Group, Huddersfield 01484 517077

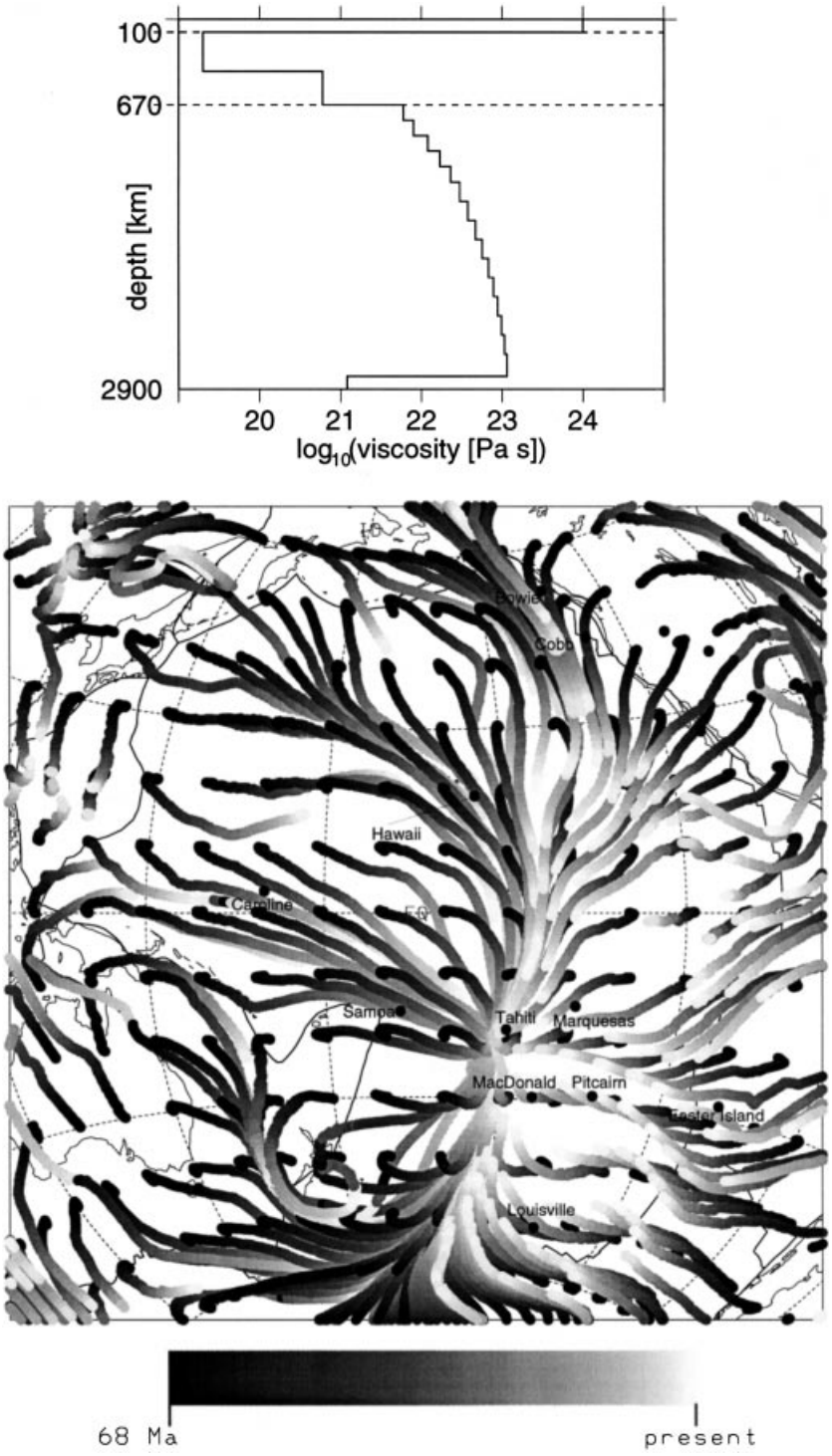

Figure 20. Hotspot motion calculated for the viscosity structure shown, eruption of plume heads at 125 Ma, otherwise as Fig. 19. Actual hotspots are shown as black dots.

hotspots under one plate at a speed of about 15 per cent of the plate velocity should be possible, and plumes should still be able to achieve the observed lifetime of over 100 Myr.

A more detailed calculation, using a more realistic 3-D flow field driven by surface plate motion and internal density heterogeneities, which were inferred from tomographic data, followed. Results of calculated hotspot motion were presented for a number of radial viscosity profiles and density heterogeneities. A relative motion which is small enough to be within the error bounds of observed hotspot fixity required a rather high viscosity of about 10^{23} Pa s for at least part of the lower mantle, if a conversion factor of 0.2 from relative seismic velocity anomalies to relative density anomalies is chosen. Coherent motion of hotspots of about 1 cm yr^{-1} over much of the Pacific Plate is compatible with such a small relative motion. As our model does not predict significant coherent

GJI000 21/1/98 16:17:18 3B2 version 5.20
The Charlesworth Group, Huddersfield 01484 517077

hotspot motion on the African Plate, it suggests an equally large motion of African Plate relative to Pacific Plate hotspots on average. The motion of the Easter hotspot relative to hotspots on the Pacific Plate could even be as large as several centimetres per year, as will be discussed in more detail in a forthcoming paper.

However, an alternative explanation was also suggested. For another model, the calculated motion of hotspots in the Pacific tends to follow certain paths, along which several of the Pacific hotspots lie: the Hawaiian, Kodiak–Bowie and Caroline hotspots. The paths converge in the central Pacific, in a region where several other hotspots are situated. If there are density heterogeneities with corresponding stationary upwellings in the mantle which are not yet resolved by tomography, plumes might be stuck along these paths in their present position, instead of getting advected all the way to the central Pacific.

The sharp bend in the Hawaiian–Emperor chain could only be reproduced if a low enough viscosity in the upper mantle was chosen. Choosing reasonable estimates for the buoyancy of the plume conduit, we obtained an upper bound of about 2×10^{20} Pa s.

Our preferred model can approximately reproduce an average lifetime similar to the estimated actual average lifetime of about 100 Myr, and lead to hotspots preferably occurring near ridges, and in regions of 'hot' (i.e. seismically slow) lower mantle, being less frequent than normal near subduction zones, just as is observed. This model implies that the motion of plume conduits at the base of the mantle is frequently larger than hotspot surface motion, thus plume conduits are often substantially tilted and the source regions of widely separated surface hotspots may be much closer.

Hotspot motions predicted from our preferred model are summarized in Fig. 21. The eruption times of the plume head were chosen according to the age of the flood basalt which the hotspot has been associated with (Richards *et al.* 1989), or the maximum age along the hotspot track (in the case of Hawaii); results do not strongly depend on them. In a forthcoming paper, implications for these and other individual hotspots will be discussed in more detail. The coherent motion of hotspots under the Pacific Plate requires revision of any plate motion model that is based on the assumption of hotspot fixity. This will also be the topic of a separate paper.

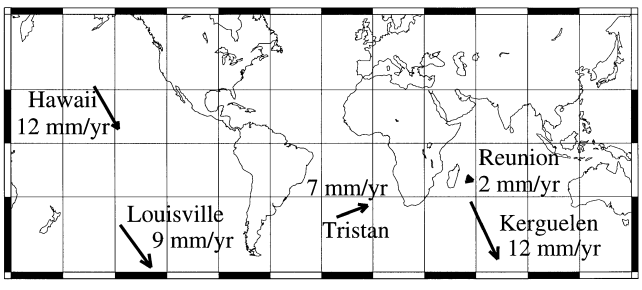

Figure 21. Predicted hotspot motions during the past 40 Myr in the no-net-rotation reference frame. Assumed eruption times of plume head: Hawaii 80 Ma; Louisville 120 Ma; Tristan 125 Ma; Reunion 67 Ma; Kerguelen 117 Ma. Mantle density heterogeneities are advected backward for 68 Ma. Otherwise same model as in Fig. 7. Total arrow length equals six times the calculated total motion since 40 Ma.

ACKNOWLEDGMENTS

Funding for this work was provided under NASA grant NAGW-3000 and NSF grant EAR-92-18923. A review by Carolina Lithgow-Bertelloni helped to improve and shorten the manuscript.

REFERENCES

Anderson, D.L., 1975. Chemical plumes in the mantle, *Geol. Soc. Am. Bull.,* **86,** 1593–1600.

Anderson, D.L., 1981. Rise of deep diapirs, *Geology,* **9,** 7–9.

Balachandar, S., Yuen, D.A., Reuteler, D.M. & Lauer, G.S., 1995. Viscous dissipation in three-dimensional convection with temperature-dependent viscosity, *Science,* **267,** 1150–1153.

Burke, K. & Wilson, J.T., 1976. Hotspots on the Earth's surface, *Sci. Am.,* **235,** 46–57.

Clague, D.A. & Dalrymple, G.B., 1989. Tectonics, geochronology, and origin of the Hawaiian-Emperor volcanic chain, in *The Geology of North America, Volume N, The Eastern Pacific Ocean and Hawaii,* pp. 188–217, eds Winterer, E.L., Hussong, D.M. & Decker, R.W., GSA, Boulder, CO.

Davies, G.F., 1988. Ocean bathymetry and mantle convection, 1, Large-scale flow and hotspots, *J. geophys. Res.,* **93,** 10 467–10 480.

DeMets, C., Gordon, R.G., Argus, D.F. & Stein, S., 1990. Current plate motions, *Geophys. J. Int.,* **101,** 425–478.

Desonie, D.L. & Duncan, R.A., 1990. The Cobb-Eickelberg seamount chain: hotspot volcanism with mid-ocean ridge basalt affinity, *J. geophys. Res.,* **95,** 12 697–12 711.

Dietz, R.S. & Holden, J.C., 1970. Reconstruction of Pangaea: Breakup and dispersion of continents, Permian to present, *J. geophys. Res.,* **75,** 4939–4956.

Duncan, R.A., 1981. Hotspots in the southern oceans—an absolute frame of reference for motion of the Gondwana continents, *Tectonophysics,* **74,** 29–42.

Duncan, R.A. & Clague, D. A., 1985. Pacific plate motion recorded by linear volcanic chains, in *The Ocean Basins and Margins,* Vol. 7a, pp. 89–121, eds Nairn, A.E.M., Stehli, F.G. & Uyeda, Plenum, New York, NY.

Dziewonski, A.M. & Anderson, D.L., 1981. Preliminary Reference Earth Model, *Phys. Earth planet. Inter.,* **25,** 297–356.

Forte, A.M., Dziewonski, A.M. & Woodward, R.L., 1993. Aspherical structure of the mantle, tectonic plate motions, nonhydrostatic geoid, and topography of the core-mantle boundary, in *Dynamics of the Earth's Deep Interior and Earth Rotation,* Geophys. Mon. Ser., Vol. 72, pp. 135–166, eds Le Mouël, J.-L., Smylie, D.E. & Herring, T., AGU, Washington, DC.

Gordon, R.G. & Jurdy, D., 1986. Cenozoic global plate motions, *J. geophys. Res.,* **91,** 12 389–12 406.

Griffiths, R.W. & Richards, M.A., 1989. The adjustment of mantle plumes to changes in plate motion, *Geophys. Res. Lett.,* **16,** 437–440.

Gripp, A.E. & Gordon, R.G., 1990. Current plate velocities relative to the hotspots incorporating the NUVEL-1 global plate motion model, *Geophys. Res. Lett.,* **17,** 1109–1112.

Hager, B.H., 1991. Mantle viscosity: A comparison of models from postglacial rebound and from the geoid, plate driving forces, and advected heat flux, in *Glacial Isostasy, Sea Level and Mantle Rheology,* pp. 493–513, eds Sabadini, R. & Lambeck, K., Kluwer Academic, Dordrecht.

Hager, B.H. & O'Connell, R.J., 1979. Kinematic models of large-scale mantle flow, *J. geophys. Res.,* **84,** 1031–1048.

Hager, B.H. & O'Connell, R.J., 1981. A simple global model of plate dynamics and mantle convection, *J. geophys. Res.,* **86,** 4843–4867.

Hewitt, J.M., McKenzie, D.P. & Weiss, N.O., 1975. Dissipative heating in convective flows, *J. Fluid Mech.,* **68,** 721–738.

GJI000 21/1/98 16:17:21 3B2 version 5.20
The Charlesworth Group, Huddersfield 01484 517077

Jarrard, R.D. & Clague, D.A., 1977. Implications of Pacific island and seamount ages for the origin of volcanic chains, *Rev. Geophys. Space Phys.,* **15,** 57–76.
Johnson, H.P. & Embley, R.W., 1990. Axial Seamount: An active ridge axis volcano on the central Juan de Fuca Ridge, *J. geophys. Res.,* **95,** 12 689–12 694.
Jurdy, D.M. & Stefanick, M., 1990. Models for the hotspot distribution, *Geophys. Res. Lett.,* **17,** 1965–1968.
Karato, S., 1993. Importance of anelasticity in the interpretation of seismic tomography, *Geophys. Res. Lett.,* **20,** 1623–1626.
Lithgow-Bertelloni, C., 1994. The history and dynamics of plate motions, *PhD thesis,* U.C. Berkeley, CA.
Lonsdale, P., 1988. Geography and history of the Louisville Hotspot Chain in the southwest Pacific, *J. geophys. Res.,* **93,** 3078–3104.
Loper, D.E. & Stacey, F.D., 1983. The dynamic and thermal structure of deep mantle plumes, *Phys. Earth planet. Inter.,* **33,** 304–317.
McKenzie, D. & O'Nions, R.K., 1983. Mantle reservoirs and ocean island basalts, *Nature,* **301,** 229–231.
Manga, M., Stone, H.A. & O'Connell, R.J., 1993. The interaction of plume heads with compositional discontinuities in the Earth's mantle, *J. geophys. Res.,* **98,** 19 979–19 990.
Molnar, P. & Stock, J., 1987. Relative motions of hotspots in the Pacific, Atlantic and Indian Ocean since late Cretaceous time, *Nature,* **327,** 587–591.
Morgan, W.J., 1971. Convection plumes in the lower mantle, *Nature,* **230,** 42–43.
Morgan, W.J., 1972. Deep mantle convection plumes and plate motions, *Am. Assoc. Petrol. Geol. Bull.,* **56,** 203–213.
Morgan, W.J., 1981. Hotspot tracks and the opening of the Atlantic and Indian Oceans, in *The Sea, Vol. 7, The Oceanic Lithosphere,* pp. 443–487, ed. Emiliani, C., Wiley, New York, NY.
Morgan, W.J., 1983. Hotspot tracks and the early rifting of the Atlantic, *Tectonophysics,* **94,** 123–139.
National Geophysical Data Center, 1988. ETOPO-5 bathymetry/topography data, *Data Announc. 88-MGG-02,* Natl. Oceanic & Atmos. Admin., US Dept Commer., Boulder, CO.
O'Connell, R.J., 1971. Pleistocene glaciation and the viscosity of the lower mantle, *Geophys. J. R. astr. Soc.,* **23,** 299–327.
O'Connell, R.J. & Hager, B.H., 1980. On the thermal state of the Earth, in *Physics of the Earth's Interior,* pp. 270–317, eds Dziewonski, A. & Boschi, E., North Holland, Amsterdam.
O'Connell, R.J., Gable, C.W. & Hager, B.H., 1991. Toroidal-poloidal partitioning of lithospheric plate motions, in *Glacial Isostasy, Sea Level and Mantle Rheology,* pp. 535–551, eds Sabadini, R. & Lambeck, K., Kluwer Academic, Dordrecht.
O'Connor, J.M., Stoffers, P. & McWilliams, M.O., 1995. Time-space mapping of Easter Chain volcanism, *Earth planet. Sci. Lett.,* **136,** 197–212.
Olson, P., 1987. Drifting mantle hotspots, *Nature,* **327,** 559–560.
Press, W.H., Flannery, B.P., Teukolski, S.A. & Vetterling, W.T., 1989. *Numerical Recipes—The Art of Scientific Computing (FORTRAN version),* Cambridge University Press, Cambridge.
Richards, M.A., 1991. Hotspots and the case against a uniform viscosity composition mantle, in *Glacial Isostasy, Sea Level and Mantle Rheology,* pp. 571–587, eds Sabadini, R. & Lambeck, K., Kluwer Academic, Dordrecht.
Richards, M.A. & Griffiths, R.W., 1988. Deflection of plumes by mantle shear flow: experimental results and a simple theory, *Geophys. J.,* **94,** 367–376.
Richards, M.A., Hager, B.H. & Sleep, N.H., 1988. Dynamically supported geoid highs over hotspots: Observation and theory, *J. geophys. Res.,* **93,** 7690–7708.
Richards, M.A., Duncan, R.A. & Courtillot, V.E., 1989. Flood basalts and hot spot tracks, *Science,* **246,** 103–107.
Sleep, N., 1990. Hotspots and mantle plumes: Some phenomenology, *J. geophys. Res.,* **95,** 6715–6736.
Steinberger, B.M., 1996. Motion of hotspots and changes of the Earth's rotation axis caused by a convecting mantle, *PhD thesis,* Harvard University, Cambridge, MA.
Su, W., Woodward, R.L. & Dziewonski, A.M., 1994. Degree 12 model of shear velocity heterogeneity in the mantle, *J. geophys. Res.,* **99,** 6945–6980.
Sumino, Y. & Anderson, O.L., 1982. Elastic constants of minerals, in *Handbook of Physical Properties of Rocks,* Vol. III, pp. 39–138, ed. Carmichael, R.S., CRC Press, Boca Raton, FL.
Watts, A.B., Weissel, J.K., Duncan, R.A. & Larson, R.L., 1988. Origin of the Louisville Ridge and its relationship to the Eltanin Fracture Zone System, *J. geophys. Res.,* **93,** 3051–3077.
Weinberg, R.F. & Podladchikov, Y., 1994. Diapiric ascent of magmas through power law crust and mantle, *J. geophys. Res.,* **99,** 9543–9559.
Wessel, P. & Smith, W.H.F., 1991. Free software helps map and display data, *EOS, Trans. Am. geophys. Un.,* **72,** 441, 445–446.
Whitehead, J.A., 1982. Instabilities of fluid conduits in a flowing earth—are plates lubricated by the asthenosphere?, *Geophys. J. R. astr. Soc.,* **70,** 415–433.
Whitehead, J.A. & Luther, D.S., 1975. Dynamics of laboratory diapir and plume models, *J. geophys. Res.,* **80,** 705–717.
Wilson, J.T., 1963. Evidence from islands on the spreading of the ocean floor, *Nature,* **197,** 536–538.

APPENDIX A: THE MANTLE FLOW FIELD

We first briefly explain the method for calculating flow in a viscous spherical shell. This flow field is needed to calculate the advection of plumes. We then explain how this method is extended to calculate the advection of mantle density heterogeneities. The advected density heterogeneities enable a more accurate calculation of mantle flow in the geological past.

A1 Method for numerical flow calculation

The method developed by Hager & O'Connell (1979, 1981) solves the following problem. Given the (plate-like) velocity distribution at the surface and the distribution of density anomalies in the interior, calculate the flow field in a spherical shell (Earth mantle), assuming Newtonian viscous rheology with viscosity depending only on radius and a free-slip boundary at the bottom (core–mantle boundary). Since we have models for both surface velocities and internal density anomalies, we can thus find a solution which automatically satisfies the known surface velocity boundary condition.

For this flow field, forces on plates do not add up to zero; it is not possible to satisfy both stress and velocity boundary conditions. However, there may be other forces acting on plates, primarily at the boundaries, which are not contained in this model and which may compensate any net forces within this model.

Models for global plate motions exist for both the present (DeMets *et al.* 1990; Gripp & Gordon 1990) and the past (Gordon & Jurdy 1986; Lithgow-Bertelloni 1994). The present distribution of density anomalies is inferred from seismic tomography. The past distribution is calculated by advecting density heterogeneities in the flow field, as described in more detail in the next section. For present density anomalies we use the tomographic model SH12/WM13 of Su *et al.* (1994). This model specifies the relative deviation $\delta v/v_0$ of seismic S-wave speed from the spherically symmetric PREM (Dziewonski & Anderson 1981).

GJI000 21/1/98 16:17:24 3B2 version 5.20
The Charlesworth Group, Huddersfield 01484 517077

In order to obtain the relative deviation $\delta\rho/\rho_0$ of density from the reference value, a conversion factor $(\delta\rho/\rho_0)/(\delta v/v_0)$ is required. Sumino & Anderson (1982) obtained a factor of about 0.4 from laboratory experiments, inherently assuming the velocity anomalies were purely thermal; however, Karato (1994) combined experimental results with theoretical considerations and obtained factors of around 0.2–0.3. By matching the results of seismic tomography with the geoid, Forte, Dziewonski & Woodward (1993) generally obtained even lower values, particularly in the lower mantle.

The flow calculation is based on the mathematical theorem that a vector field $\mathbf{v}(\mathbf{r})$ defined on a spherical shell can be expressed in spherical coordinates in terms of three scalar fields u_1, u_2 and w_1 in the following way:

$$\mathbf{v} = \mathbf{e}_r \cdot u_1 + \nabla u_2 - \mathbf{e}_r \times \nabla \cdot w_1 \,. \tag{A1}$$

Using co-latitude θ and longitude ϕ as coordinates, u_1, u_2 and w_1 can be expressed in terms of fully normalized spherical harmonics $\bar{Y}_{lm}$, thus it is possible to write the velocity components in radial, southerly and easterly directions, v_r, v_θ and v_ϕ, in the form

$$\begin{aligned} v_r &= \sum_{l=0}^{\infty} \sum_{m=-l}^{l} u_{1,lm} \bar{Y}_{lm} \,, \\ v_\theta &= \sum_{l=0}^{\infty} \sum_{m=-l}^{l} u_{2,lm} \frac{\partial \bar{Y}_{lm}}{\partial \theta} + w_{1,lm} \frac{1}{\sin\theta} \frac{\partial \bar{Y}_{lm}}{\partial \phi} \,, \\ v_\phi &= \sum_{l=0}^{\infty} \sum_{m=-l}^{l} u_{2,lm} \frac{1}{\sin\theta} \frac{\partial \bar{Y}_{lm}}{\partial \phi} + w_{1,lm} \frac{\partial \bar{Y}_{lm}}{\partial \theta} \,. \end{aligned} \tag{A2}$$

Similarly one may express the components τ_{rr}, $\tau_{r\theta}$ and $\tau_{r\phi}$ of the non-hydrostatic stress tensor $\boldsymbol{\tau}$, which specify the force per area on a horizontal surface, in radial, southerly and easterly directions, in the form

$$\begin{aligned} \tau_{rr} &= \frac{\eta_0}{r} \sum_{l=0}^{\infty} \sum_{m=-l}^{l} u_{3,lm} \bar{Y}_{lm} \,, \\ \tau_{r\theta} &= \frac{\eta_0}{r} \sum_{l=0}^{\infty} \sum_{m=-l}^{l} u_{4,lm} \frac{\partial \bar{Y}_{lm}}{\partial \theta} + w_{2,lm} \frac{1}{\sin\theta} \frac{\partial \bar{Y}_{lm}}{\partial \phi} \,, \\ \tau_{r\phi} &= \frac{\eta_0}{r} \sum_{l=0}^{\infty} \sum_{m=-l}^{l} u_{4,lm} \frac{1}{\sin\theta} \frac{\partial \bar{Y}_{lm}}{\partial \phi} + w_{2,lm} \frac{\partial \bar{Y}_{lm}}{\partial \theta} \,, \end{aligned} \tag{A3}$$

where η_0 is the constant normalizing viscosity and r is the radius. The deviation $\delta\varphi$ of the gravity potential from the reference value, its radial derivative $\partial\delta\varphi/\partial r$ as well as density anomalies $\delta\rho$ may also be expanded in spherical harmonics; one may thus write

$$\begin{aligned} \delta\varphi &= \frac{\eta_0}{\rho_{00} r} \sum_{l=0}^{\infty} \sum_{m=-l}^{l} u_{5,lm} \bar{Y}_{lm} \,, \\ \frac{\partial \delta\varphi}{\partial r} &= \frac{\eta_0}{\rho_{00} r^2} \sum_{l=0}^{\infty} \sum_{m=-l}^{l} u_{6,lm} \bar{Y}_{lm} \,, \\ \delta\rho &= \sum_{l=0}^{\infty} \sum_{m=-l}^{l} \delta\rho_{lm} \bar{Y}_{lm} \,, \end{aligned} \tag{A4}$$

where ρ_{00} is the constant normalizing density.

Summation is only performed up to degree and order Λ. In order to evaluate these sums, the order of summation is reversed: For example,

$$v_r(\theta, \phi) = \sum_{m=-\Lambda}^{\Lambda} \sum_{l=|m|}^{\Lambda} u_{1,lm} \bar{Y}_{lm}(\theta, \phi) \,, \tag{A5}$$

and entirely analogous rearrangements of the other sums. Summation is therefore performed in two steps. First, for each value of m and each value of θ the second sum is calculated. This sum is independent of ϕ, therefore this step requires $O(N\Lambda^2)$ operations if the expansion is carried out on a 2-D grid of $2N \times N$ points. Second, the outer sum is calculated for each value of θ and ϕ. This step requires $O(N^2\Lambda)$ operations. The total number of operations has thus been significantly reduced compared to directly evaluating the double sums (A2)–(A4).

Following Hager & O'Connell (1979), with these expansions the equations governing the flow can be solved separately for each spherical harmonic. After omitting the indices lm and combining $u_1 \ldots u_6$ to a vector $\mathbf{u}$ and w_1 and w_2 to a vector $\mathbf{w}$, they can be brought into the form

$$\frac{d\mathbf{u}}{dr} = \frac{1}{r} \mathbf{A} \cdot \mathbf{u} + \mathbf{b}, \qquad \frac{d\mathbf{w}}{dr} = \frac{1}{r} \mathbf{B} \cdot \mathbf{w} \,, \tag{A6}$$

with

$$\mathbf{A} = \begin{pmatrix} -2 & L & 0 & 0 & 0 & 0 \\ -1 & 1 & 0 & 1/\eta^* & 0 & 0 \\ 12\eta^* & -6L\eta^* & 1 & L & 0 & -\rho^* \\ -6\eta^* & 2(2L-1)\eta^* & -1 & -2 & -\rho^* & 0 \\ 0 & 0 & 0 & 0 & 1 & 1 \\ 0 & 0 & 0 & 0 & L & 0 \end{pmatrix},$$

$$\mathbf{b} = \begin{pmatrix} 0 \\ 0 \\ \dfrac{r^2 \delta\rho g}{\eta_0} \\ 0 \\ 0 \\ \dfrac{-4\pi r^3 \rho_{00} G \delta\rho}{\eta_0} \end{pmatrix}, \tag{A7}$$

$$\mathbf{B} = \begin{pmatrix} 1 & 1/\eta^* \\ (L-2)\eta^* & -2 \end{pmatrix}. \tag{A8}$$

$L = l(l+1)$, $\eta^* = \eta/\eta_0$, η is viscosity, $\rho^* = \rho_0/\rho_{00}$, g is gravity acceleration and G is the gravitation constant. These systems of ordinary differential equations are solved with a propagator matrix technique for a spherical shell consisting of layers of constant viscosity.

The mantle flow field is modelled as consisting of a kinematic and a density-driven part. The coefficients of the kinematic flow field are calculated from the surface velocity field of the plates, assuming no internal density variations. This means we set $\mathbf{b}$ equal to zero in eq. (A6), expand the

GJI000 21/1/98 16:17:31 3B2 version 5.20
The Charlesworth Group, Huddersfield 01484 517077

given surface plate velocities in spherical harmonics and use the expansion coefficients as boundary conditions in eq. (A6).

The coefficients of the density-driven flow field are calculated from given density anomalies in the mantle, assuming zero velocity at the surface. The sum of both flow fields satisfies both the equations of fluid flow in a mantle of laterally heterogeneous density and the velocity boundary condition at the surface.

For a given density and surface velocity field, the resulting mantle flow field depends strongly on the radial viscosity structure. If the lower mantle is not decoupled from the surface plates by a zone of low viscosity, the flow is related to the motion of the surface plates, with upwellings near ridges and downwellings near trenches. If, however, a zone of low viscosity exists, the flow in the lower mantle is almost entirely determined by the internal density structure, and therefore shows less relation to features at the surface.

A2 Advection of mantle density heterogeneities

In order to model the flow field in the geological past more accurately, we calculate time changes of the density field and thus the past density field. Hereby we make the basic assumption that density anomalies are of purely thermal origin and thus the relation to temperature anomalies is $\delta\rho/\rho_0 = \alpha\delta T$, where α is the thermal expansion coefficient. δT is the difference between the actual temperature, T, and the radially symmetric and time-independent reference temperature $T_0(r)$, and changes of T with time follow from the general equation of heat transfer, which for constant thermal conductivity K may be written in the form

$$\rho C_p \frac{\partial T}{\partial t} = -\rho C_p \mathbf{v}\cdot(\nabla T - \nabla T_s) + \boldsymbol{\tau}\cdot\boldsymbol{\epsilon} + K\nabla^2 T + A\,, \tag{A9}$$

where C_p is heat capacity at constant pressure, ∇T_s is the adiabatic temperature gradient and $\boldsymbol{\epsilon}$ is the strain tensor (O'Connell & Hager 1980, eq. 7). The terms on the right-hand side have the following meaning. $\boldsymbol{\tau}\cdot\boldsymbol{\epsilon}$ is due to viscous dissipation; using the stress–strain relationship, we find

$$\boldsymbol{\tau}\cdot\boldsymbol{\epsilon} = 4\eta(\epsilon_{\phi\phi}\epsilon_{\phi\phi} + \epsilon_{\phi\theta}\epsilon_{\phi\theta} + \epsilon_{\theta\theta}\epsilon_{\theta\theta} + \epsilon_{\phi\phi}\epsilon_{\theta\theta}) + \frac{1}{\eta}(\tau_{\phi r}\tau_{\phi r} + \tau_{\theta r}\tau_{\theta r})\,, \tag{A10}$$

which can be expressed in a fully analytical way through eqs (A2) and (A3). $K\nabla^2 T$ is due to heat conduction and A is due to heat production. After making the further assumption (approximately true outside the thermal boundary layers) that $T_0(r)$ is adiabatic, the first term can be split into two parts:

$$\begin{aligned} &-\rho C_p \mathbf{v}\cdot(\nabla T - \nabla T_s) \\ &\quad = -\rho C_p \mathbf{v}\cdot(\nabla T - \nabla T_0) + \rho C_p \mathbf{v}\cdot(\nabla T_s - \nabla T_0) \\ &\quad = -\rho C_p \mathbf{v}\cdot\nabla\delta T + \rho C_p \mathbf{v}\cdot(\alpha T g/C_p \mathbf{e}_z - \alpha T_0 g/C_p \mathbf{e}_z) \\ &\quad = -\rho C_p \mathbf{v}\cdot\nabla\delta T + \rho v_z \alpha\delta T g\,. \end{aligned} \tag{A11}$$

The first part is due to advection of heat. The second part results from the fact that hot upwellings cool off more during adiabatic decompression than cold downwelling heat up during adiabatic compression; when integrated over the entire Earth it exactly cancels the contribution of viscous heating (Hewitt, McKenzie & Weiss 1975).

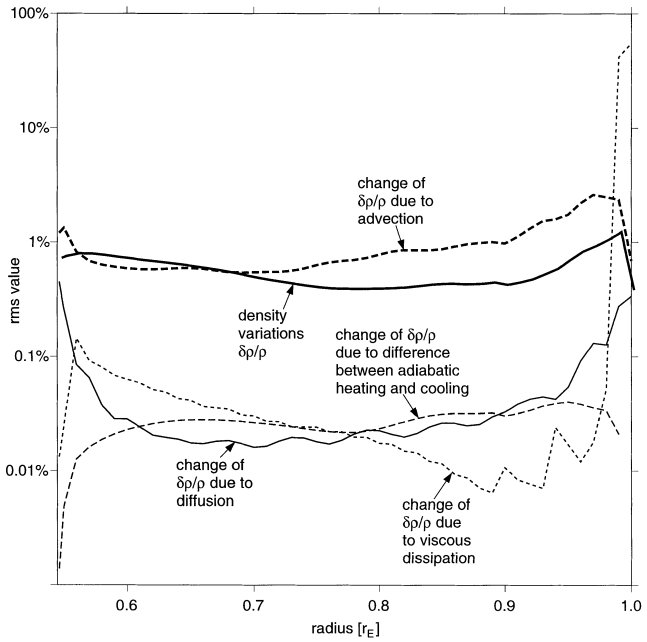

Figure A1. Root mean square values of mantle density relative variations $\delta\rho/\rho$, and the components of its normalized time change $\partial(\delta\rho/\rho)/\partial t \times 68$ Myr due to advection, heat diffusion (valid outside thermal boundary layers), viscous heating, as well as the difference between adiabatic heating and cooling as a function of radius for the preferred model at the present day. Hereby we adopt constant numerical values representative for mantle rocks: $C_p = 10^3$ J kg^{-1} K^{-1}, $\kappa = 1.2\times10^{-6}$ m^2 s^{-1}, $\alpha = 10^{-5}$ K^{-1}.

It has been argued that the temperature dependence of viscosity can lead to large viscous dissipation (Balachandar *et al.* 1995). For the large-scale flow field discussed here, however, this is not the case: Fig. A1 shows that the rms value of density change due to viscous heating is much

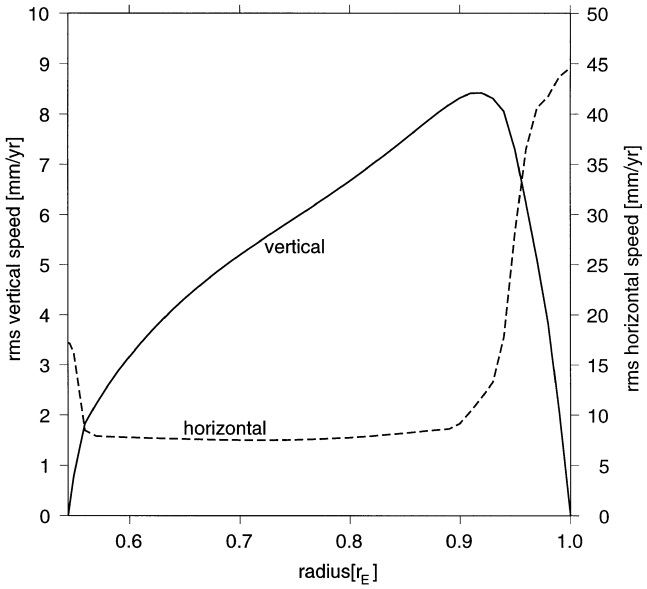

Figure A2. Root mean square values of horizontal and vertical mantle flow velocity as a function of radius for the preferred model at the present day. For clarity the vertical scale is different for both curves.

GJI000 21/1/98 16:18:11 3B2 version 5.20
The Charlesworth Group, Huddersfield 01484 517077

smaller than the change due to advection, except near the upper boundary (the latter is a numerical artefact—the plate-like velocity boundary condition in combination with the high viscosity yields a very high dissipation near the plate boundaries). Also, the viscous dissipation term and the difference between adiabatic heating and cooling are much smaller than the advective term, except in the boundary layers, where the equations are not valid. Thus we may approximately neglect these terms as long as the volume fraction of mantle that enters or leaves the thermal boundary layers is negligible. From Fig. A2 it can be inferred that during 68 Myr a significant fraction of the upper mantle volume, but only a small fraction of the lower mantle, may move into or out of the thermal boundary layers. We therefore conclude that for our purposes it is a valid approximation to neglect these terms when calculating the density and flow field during the past 68 Myr. This is especially true as we show that plumes and hotspots are more strongly affected by flow and hence density anomalies in the lower mantle. However, the calculation will be less reliable the further back in time we go. If we assume the mantle does not heat up or cool down on average, heat production will equal heat loss due to diffusion, hence we may neglect the heat-production term as well.

Under the assumptions made, the density change at any fixed location is only due to advection. If we additionally assume $\alpha\rho_0$ is constant with depth, we may write

$$\frac{\partial \delta\rho}{\partial t} = -\nabla \delta\rho \cdot \mathbf{v}, \tag{A12}$$

and thus advect the density heterogeneities backward in time.

Flow is calculated from density anomalies and surface plate motion in terms of spherical harmonics according to (A6); to perform the multiplication of velocity and density gradient, these fields are evaluated on a grid of 2^n points in latitude, 2^{n+1} points in longitude and m radial points. For the latitudes, we choose the points of the Gauss–Legendre quadrature formula; in longitude the points are equally spaced, thus enabling a re-expansion in terms of spherical harmonics. Time integration of density is carried out with a fourth-order Runge–Kutta scheme (Press *et al.* 1989).

GJI000 21/1/98 16:18:32 3B2 version 5.20
The Charlesworth Group, Huddersfield 01484 517077